Current injection efficiency of InGaAsN quantum-well lasers

Nelson Tansu[a)]
Department of Electrical and Computer Engineering, Center for Optical Technologies, Lehigh University, 7 Asa Drive, Bethlehem, Pennsylvania 18015

Luke J. Mawst
Department of Electrical and Computer Engineering, Reed Center for Photonics, University of Wisconsin-Madison, 1415 Engineering Drive, Madison, Wisconsin 53706

(Received 3 August 2004; accepted 30 November 2004; published online 9 February 2005)

The concept of below-threshold and above-threshold current injection efficiency of quantum well (QW) lasers is clarified. The analysis presented here is applied to the current injection efficiency of 1200 nm emitting InGaAs and 1300 nm emitting InGaAsN QW lasers. The role of heavy-hole leakage in the InGaAsN QW lasers is shown to be significant in determining the device temperature sensitivity. The current injection efficiency of QW lasers with large monomolecular recombination processes is shown to be less temperature sensitive. Excellent agreement between theory and experiment is obtained for both the 1200 nm emitting InGaAs QW and the 1300 nm emitting InGaAsN QW lasers. Suppression of thermionic carrier escape processes in the InGaAsN QW results in high performance 1300 nm emitting lasers operating up to high temperature. © *2005 American Institute of Physics*. [DOI: 10.1063/1.1852697]

I. INTRODUCTION

The early InGaAsN quantum-well (QW) lasers have typically displayed very high threshold-current density (J_{th}) and anomalously high T_0 [$1/T_0=(1/J_{th})dJ_{th}/dT$] values, presumably due to the large monomolecular recombination present.[1,2] Recently, high-performance InGaAsN quantum-well lasers have been realized both by metalorganic chemical vapor deposition and molecular beam epitaxy.[1–12] Unfortunately, the T_0 values of the high-performance 1300 nm emitting InGaAsN single-QW lasers are only in the range 70–110 K,[1–12] which is low compared to optimized 1200 nm emitting InGaAs single-QW lasers ($T_0=200$ K).[13–15]

There have been studies, without taking into account carrier leakage, which has suggested the existence of large Auger recombination processes in the 1300 nm emitting InGaAsN QW lasers.[2] From our studies,[1,16] we have shown that carrier leakage cannot be neglected in InGaAsN QW lasers due to the possibility of hole leakage out of the QW.[2] In this work, the reduction of T_0 and T_1 values of the 1300 nm emitting InGaAsN QW lasers, in comparison to those of the 1200 nm emitting InGaAs QW lasers, has been attributed to larger carrier/current leakage processes and a more temperature sensitive material gain parameter.[1] Despite the deeper well structure in the InGaAsN QW lasers, its experimentally measured above-threshold current injection efficiency (η_{inj}) reduces more rapidly with temperature compared to that of the 1200 nm InGaAs QW lasers.[1] The strong temperature dependence of the current injection efficiency of InGaAsN QW lasers indicates there may exist significantly increased thermionic emission of carriers out of the QW at elevated temperature.[16] An improved understanding of the carrier transport and current injection efficiency in InGaAsN QW lasers will provide enlightenment to the understanding of carrier leakage processes in InGaAsN QWs, despite its significantly stronger electron confinement.

The aim of this work is to identify and explain the behavior of the carrier/current injection efficiencies in the 1200 nm emitting InGaAs QW and 1300 nm emitting InGaAsN QW lasers. Here we will present a detailed analysis[17] of the below-threshold, at-threshold, and above-threshold current injection efficiency (η_{inj}) of single quantum well lasers, taking into account the recombination in the QW, recombination in the barriers (SCH), carrier transport, and capture effect, and thermionic carrier escape effects. The analysis presented here is valid for any type of quantum-well laser.[17] However, we will apply this analysis for the understanding of the current injection efficiency of both the 1200 nm emitting InGaAs QW and 1300 nm emitting InGaAsN QW lasers. Design parameters for obtaining high η_{inj} and temperature insensitive η_{inj} [i.e., large $T_{\eta inj}$ value, $1/T_{\eta inj}=-(1/\eta_{inj})(d_{\eta inj}/dT)$] will also be presented. The role of nonradiative recombination in QW lasers in relation to the above- and below-threshold current injection efficiency will also be clarified. We find that the higher temperature sensitivity of the η_{inj} for InGaAsN QW lasers can be understood from an increase in heavy-hole leakage, due to the smaller hole confinement in the InGaAsN QW lasers. Excellent agreement between theory and experiments is obtained for both the 1300 nm emitting InGaAsN QW and the 1200 nm emitting InGaAs QW lasers. Design analysis with larger-band gap barriers and multiquantum well (MQW) structures for reduced sensitivity of current injection efficiency will also be presented. Experiments on InGaAsN QW lasers with large band gap GaAsP barriers, to suppress the thermionic hole leakage, result in very low threshold current density at elevated temperature. Utilizing GaAsP barriers in InGaAsN QW lasers also leads to the realization of InGaAsN QW

[a)]Author to whom correspondence should be addressed; electronic mail: tansu@lehigh.edu

lasers with temperature-insensitive slope efficiency at elevated temperature, confirming the predictions of our model.

The concept of current injection efficiency in QW lasers will be discussed in Sec. II. The theoretical model of the current injection efficiency of QW lasers will be derived in Sec. III. Once the parameters of interest for the current injection efficiency model have been discussed in detail in Sec. IV, we will present the analysis of the thermionic carrier escape processes in InGaAs QW and InGaAsN QW lasers in Sec. V. Simulation results of the carrier transport and current injection efficiencies of both 1200 nm emitting InGaAs and 1300 nm emitting InGaAsN QW lasers will be presented in Sec. VI. Impact of the carrier leakage on the lasing characteristics of InGaAs and InGaAsN QW lasers will be presented in Sec. VII. Experiments to confirm the existence of carrier leakage and the importance of suppressing thermionic carrier escape processes in InGaAsN QW lasers with large band gap barrier materials will be presented in detail in Sec. VIII.

II. CONCEPT OF CURRENT INJECTION EFFICIENCY

A. Definitions and understanding

The concept of the current injection efficiency of QW lasers is often misunderstood.[18–22,48] The current injection efficiency of QW lasers has been typically assumed to be the same for the cases of below-threshold, at-threshold, and above-threshold conditions. The conventional approach in extracting the current injection efficiency of QW lasers is by utilizing a multiple cavity length study.[19–23] As pointed out by Smowton and Blood[18] for the case of visible-wavelength InGaP QW lasers, the at-threshold (including below-threshold) and above-threshold current injection efficiency can have very distinct values. In general, the at-threshold and above-threshold current injection efficiency of QW lasers are conceptually very different.[21,23] Typically the current injection efficiency of a properly designed double heterostructure laser is similar for both the above and at-threshold conditions. However, as the dimensionality of the active region is reduced, the at-threshold and above-threshold current injection efficiency of the active region cannot be assumed as similar.

The current injection efficiency (η_{inj}) of QW lasers is defined as the fraction of the injected current that recombines, both radiatively and nonradiatively, in the QW-active region of the laser. The current injection efficiency (η_{inj}) is distinct from the internal efficiency (η_i), as the internal efficiency is defined as the fraction of the injected current that recombines radiatively in the QW-active region.[48] The relationship between the internal efficiency and the current injection efficiency can be written as follows:

$$\eta_i = \eta_{\mathrm{inj}} \cdot \eta_{\mathrm{Quantum\_Efficiency}}, \tag{1}$$

in which the $\eta_{\mathrm{Quantum\_Efficiency}}$ $(=R_{\mathrm{rad}}/R_{\mathrm{total}})$ is defined as the fraction of the total recombination in QW ($R_{\mathrm{total}}=R_{\mathrm{rad}}+R_{\mathrm{non\text{-}rad}}$) that recombine radiatively (R_{rad}). The nonradiative recombination in QW ($R_{\mathrm{non\text{-}rad}}$) may consist of recombination through monomolecular or Auger processes.

The current injection efficiency (η_{inj}) consists of the structural current injection efficiency ($\eta_{\mathrm{inj\_structure}}$) and the current injection efficiency of the QW ($\eta_{\mathrm{inj\_QW}}$), which can be expressed as follows:

$$\eta_{\mathrm{inj}\_X} = \eta_{\mathrm{inj\_structure}} \cdot \eta_{\mathrm{inj\_QW}\_X}, \tag{2}$$

where X represents the below-threshold (below_th), at-threshold (at_th), or above-threshold (above_th) conditions. For the discussion presented here, the $\eta_{\mathrm{inj\_structure}}$ is assumed as constant for a limited temperature regime. This assumption is typically very good for wide-stripe lasers with a stripe width (w) of many times the diffusion length, as the lateral current spreading and diffusion in broad-area lasers are fixed for a given structure. The $\eta_{\mathrm{inj\_structure}}$ will also play a role in the lasers which have poor interfaces outside of the QW-active region or separate-confining heterostructure (SCH) barrier regions, as the carrier losses at the poor interfaces in the cladding layers will lead to a reduction of the $\eta_{\mathrm{inj\_structure}}$. For broad-area ($w=100\ \mu$m) lasers with identical SCH structures [i.e., only the active regions (InGaAs QW or InGaAsN QW) are changed], the assumption of the constant $\eta_{\mathrm{inj\_structure}}$ should be valid. Therefore, for the study presented here, the $\eta_{\mathrm{inj\_QW}}$ is the parameter of interest in most cases. The $\eta_{\mathrm{inj\_QW}}$ will be analyzed both for the below- and above-threshold conditions, at various temperatures (T) and carrier concentrations in the QW (N_{QW}). From our analysis, we find that the properties of both the below-threshold and above-threshold $\eta_{\mathrm{inj\_QW}}$ are very distinct for the 1200 nm InGaAs and the 1300 nm InGaAsN QW lasers, with similar SCH structures.

B. The below-and at-threshold conditions

The threshold current density of semiconductor lasers can be expressed as functions of the physical parameters as follows:

$$J_{\mathrm{th}} = \frac{J_{\mathrm{tr}}}{\eta_{\mathrm{inj\_at\_threshold}}} \cdot \exp\left(\frac{\alpha + (1/L)\ln(1/R)}{\Gamma g_{oJ}}\right), \tag{3}$$

with J_{tr}, $\eta_{\mathrm{inj\_at\_threshold}}$, g_{oJ}, and α_i, as transparency current density, at-threshold current injection efficiency, material gain parameters, and internal loss, respectively. The mirror loss $\alpha_m(L)$ is expressed as $(1/L)\ln(1/R)$. The below-threshold ($\eta_{\mathrm{inj\_QW\_below\_th}}$) and at-threshold ($\eta_{\mathrm{inj\_QW\_th}}$) current injection efficiency of QW lasers represent the fraction of the injected current which recombines in the QW-active region, before the laser reaches the lasing threshold condition. These values depend on the details of the structure, carrier density, and temperature.

C. The above-threshold condition

The output power of semiconductor lasers can be expressed as a function of the physical parameters as follows:

$$P_{\mathrm{output}} = \eta_{\mathrm{diff\_ext}} \cdot (J - J_{\mathrm{th}}) \cdot A \cdot \frac{E_p}{q}, \tag{4}$$

with the J, J_{th}, $\eta_{\mathrm{diff\_ext}}$, and A as the injected and threshold current density, external differential efficiency, and area of the laser stripe, respectively. The E_p and q correspond to the photon energy of the lasing wavelength and the electron charge, respectively. The external differential efficiency ($\eta_{\text{diff\_ext}}$) can be expressed as

$$\eta_{\text{diff\_ext}} = \eta_{\text{inj\_above\_th}} \cdot \frac{\alpha_m(L)}{\alpha_i + \alpha_m(L)}. \tag{5}$$

The $\eta_{\text{inj\_above\_th}}$ is the differential fraction of the injected current that recombines in the QW, after the lasing phenomena occurs. The modal gain is clamped in the QW at threshold and above threshold, but this does not necessarily lead to full clamping of carriers in the QW or SCH regions above threshold.[18,21,23] The $\eta_{\text{inj\_above\_th}}$ can be very different from the at-threshold current injection efficiency, as a result of the full or partial clamping phenomena of carriers in the QW above threshold. It is important to clarify that from conventional length studies, a measurement of $\eta_{\text{diff\_ext}}$ for various cavity-length devices will only result in the extraction of $\eta_{\text{inj\_above\_th}}$ and α_i (i.e., not $\eta_{\text{inj\_below\_th}}$).

III. MODEL OF CURRENT INJECTION EFFICIENCY

In modeling the current injection efficiency, the parameter of interest is the current injection efficiency of the QW-active region ($\eta_{\text{inj\_QW}}$). Any fraction of current/carrier loss from poor interfaces in the cladding layers or lateral current diffusion from the contact region will be accounted for in the $\eta_{\text{inj\_structure}}$. Therefore, the injected current into the SCH (I_{SCH}) will be equivalent to $\eta_{\text{inj\_structure}}$ ($=I_{\text{SCH}}/I_{\text{total}}$) times the total injected current (I_{total}) into the laser device. The I_{SCH} consists of a combination of the injected current from the n-cladding ($I_{\text{SCH\_}n}$) and the p-cladding ($I_{\text{SCH\_}p}$) layers.

To realize a physically intuitive model of the current injection efficiency of the QW-active region, without having to utilize a complex numerical solution of the problem, we utilize a three-level rate equation model.[23] The model that we employ here consists of the rate equations for the carrier density in the QW-active region (N_{QW}), carrier density in the SCH-barrier region (N_B), and the photon density (S). The variation in the carrier density along the length of the active region has been neglected, as the variation in the longitudinal direction for QW lasers is not significant for lasers with facet reflectivity larger than 20%.[24] The carrier density variation in the lateral direction is also negligible, as the stripe width is many times the diffusion length.

The three rate equations for carrier density and photon density in electrically injected QW lasers can be expressed as follows:

$$\frac{dN_{\text{QW}}}{dt} = \frac{N_B \cdot (V_B/V_{\text{QW}})}{\tau_{\text{bw}}} - N_{\text{QW}} \cdot \left(\frac{1}{\tau_{\text{QW\_rad}}} + \frac{1}{\tau_{\text{QW\_non\_rad}}} + \frac{1}{\tau_e} \right) - \frac{\nu_g \cdot g(N_{\text{QW}}) \cdot S}{(1 + \varepsilon \cdot S)}, \tag{6}$$

$$\frac{dN_B}{dt} = \frac{I_{\text{SCH}}}{qV_B} - N_B \cdot \left(\frac{1}{\tau_b} + \frac{1}{\tau_{\text{bw}}} \right) + \frac{N_{\text{QW}} \cdot (V_{\text{QW}}/V_B)}{\tau_e}, \tag{7}$$

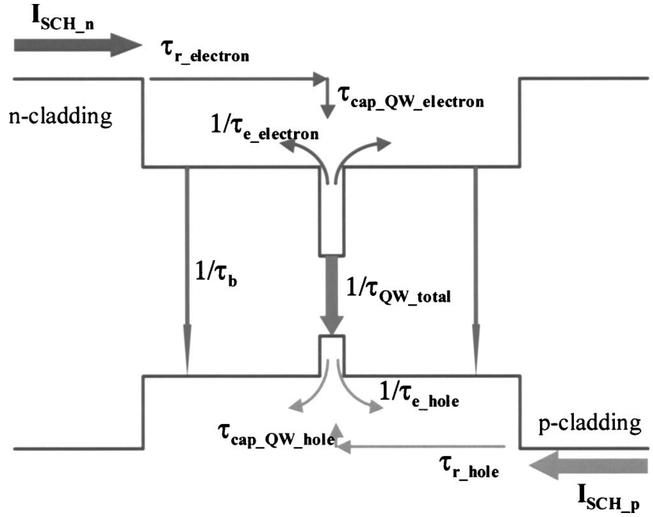

FIG. 1. Schematic of the single-QW lasers used in the model for current injection efficiency.

$$\frac{dS}{dt} = \frac{\Gamma \cdot \nu_g \cdot g(N_{\text{QW}}) \cdot S}{(1 + \varepsilon \cdot S)} - \frac{S}{\tau_p} + \frac{\Gamma \cdot \beta \cdot N_{\text{QW}}}{\tau_{\text{QW\_rad}}}, \tag{8}$$

where τ_{bw} is the total carrier capture time from the SCH/barrier to QW, $\tau_{\text{QW\_rad}}$ is the radiative recombination lifetime in the QW, $\tau_{\text{QW\_non\_rad}}$ is the monomolecular and Auger nonradiative recombination lifetime in the QW, τ_e is the carrier thermionic emission escape time from the QW to the barrier region, τ_b is the total recombination lifetime of the carriers in the barrier/SCH region, τ_p is the photon lifetime, V_{QW} is the volume of the QW, V_{SCH} is the volume of the barrier/SCH region, Γ is the transverse optical confinement factor, ν_g is the group velocity of the mode, $g(N_{\text{QW}})$ is the peak gain provided by the carriers in the QW, ε is the intrinsic gain compression factor, and β is the spontaneous emission coupling to the lasing mode. An illustration of the transverse direction of the laser is shown in Fig. 1. Although the rate equation treatment presented here ignores the fact that the electron and holes are injected from different cladding regions, a more in-depth analysis taking account this fact has yielded essentially similar result for studies concerning the dynamics of high speed lasers.[21,23,25] Even though the analysis of interest here will be utilized to analyze only the case of single QW lasers, this analysis can be easily extended for the case of multiple QW lasers, as will be discussed later.

Both the radiative and the nonradiative recombination processes in the QW are important factors in determining the temperature sensitivity of the $\eta_{\text{inj\_QW}}$. The total recombination lifetime in the QW ($\tau_{\text{QW\_total}}$) can be expressed as $1/\tau_{\text{QW\_total}} = 1/\tau_{\text{QW\_rad}} + 1/\tau_{\text{QW\_non\_rad}}$. The photon lifetime τ_p is the inverse of the total cavity loss rate, which can be expressed as follows: $\tau_p = 1/[\nu_g(\alpha_i + \alpha_m)]$. The $1/\tau_e$ value represents the thermionic escape rate of carriers from the QW into the barriers. A larger carrier escape rate from QW will also lead to overflow of carriers in the barrier/SCH region. In our analysis, both the electron and hole thermionic escape time will be calculated, which will be elaborated on later.

The τ_{bw} ($=\tau_{\text{cap\_QW}} + \tau_r$), in general, consists of the quantum mechanical capture time into the QW ($\tau_{\text{cap\_QW}}$) and transport time from the edge of the SCH to the QW (τ_r). Nagarajan and co-workers[25] have shown that τ_r dominates to $\tau_{\text{cap\_QW}}$ for typical QW lasers, both theoretically and experimentally, in the carrier capture process from barriers into QW. The typical $\tau_{\text{cap\_QW}}$ will range from 0.3 to 0.5 ps for QW lasers,[26] which is significantly smaller than the typical transport time of holes ($\tau_r \sim 5$–6 ps) in QW lasers.[23,25,27] In our analysis here, only the τ_r will be considered in the τ_{bw}, though $\tau_{\text{cap\_QW}}$ can be incorporated as needed into the equation without any loss in generality.

In the analysis here, only the steady-state (dc) conditions are of interest. By taking the time derivative of Eqs. (6)–(8) to be zero, the following conditions can be achieved as follows:

$$\frac{I_{\text{SCH}}}{q} = N_B V_B \cdot \left(\frac{1}{\tau_b} + \frac{1}{\tau_{\text{bw}}}\right) - \frac{N_{\text{QW}} \cdot V_{\text{QW}}}{\tau_e}, \tag{9}$$

$$N_B = \tau_{\text{bw}} \cdot \frac{V_{\text{QW}}}{V_B} \cdot \left[N_{\text{QW}} \cdot \left(\frac{1}{\tau_e} + \frac{1}{\tau_{\text{QW\_total}}}\right) + \frac{\nu_g \cdot g(N_{\text{QW}}) \cdot S}{1 + \varepsilon \cdot S} \right], \tag{10}$$

$$\frac{1}{\tau_p} = \frac{\Gamma \cdot \nu_g \cdot g(N_{\text{QW}})}{1 + \varepsilon \cdot S} + \frac{\Gamma \cdot \beta \cdot N_{\text{QW}}}{\tau_{\text{QW\_total}} \cdot S}. \tag{11}$$

The total recombination current in the QW ($I_{\text{QW\_total}}$) can be expressed as $I_{\text{QW\_total}} = N_{\text{QW}} \cdot V_{\text{QW}} \cdot q / \tau_{\text{QW\_total}}$. By relating Eqs. (9) and (10), the relation of the I_{SCH} to the $I_{\text{QW\_total}}$ can be obtained as follows:

$$I_{\text{SCH}} = I_{\text{QW\_total}} \cdot \left[1 + \frac{\tau_{\text{bw}}}{\tau_b} \cdot \left(1 + \frac{\tau_{\text{QW\_total}}}{\tau_e}\right) + \tau_{\text{bw}} \cdot \frac{\tau_{\text{QW\_total}}}{N_{\text{QW}}} \cdot \frac{\nu_g \cdot g(N_{\text{QW}}) \cdot S}{1 + \varepsilon \cdot S} \right]. \tag{12}$$

The current injection efficiency of the QW for below-threshold and at-threshold ($\eta_{\text{inj\_QW\_below\_th}} = I_{\text{QW\_total}} / I_{\text{SCH}}$) can be expressed as follows:

$$\eta_{\text{inj\_QW\_below\_th}} = \frac{1}{\left[1 + \frac{\tau_{\text{bw}}}{\tau_b} \cdot \left(1 + \frac{\tau_{\text{QW\_total}}}{\tau_e}\right) + \tau_{\text{bw}} \cdot \frac{\tau_{\text{QW\_total}}}{N_{\text{QW}}} \cdot \frac{\nu_g \cdot g(N_{\text{QW}}) \cdot S}{1 + \varepsilon \cdot S} \right]}. \tag{13}$$

For the below-threshold and at-threshold condition, the photon density (S) in the cavity is typically minimal; thus the last term in the denominator of Eq. (13) can be neglected in the below-threshold and at-threshold calculation, resulting in a simpler form as follows:

$$\eta_{\text{inj\_QW\_below\_th\_\&\_at\_th}}(S \to 0) \cong \frac{1}{\left[1 + \frac{\tau_{\text{bw}}}{\tau_b} \cdot \left(1 + \frac{\tau_{\text{QW\_total}}}{\tau_e}\right) \right]}. \tag{14}$$

Equation (14) derived here is the general equation for current injection efficiency for the below- and at-threshold conditions. An analogous equation has also been derived by Nagarajan and co-workers[23] for the special case of below-threshold internal efficiency without any nonradiative processes ($1/\tau_{\text{QW\_non\_rad}} \to 0$). All the parameters τ_{bw}, τ_b, $\tau_{\text{QW\_total}}$, and τ_e are functions of the carrier density in the QW and temperature, specific to each QW-active region under study. A large thermionic carrier escape rate will lead to a reduction in τ_e and τ_b, which will in turn lead to severe degradation of the $\eta_{\text{inj\_QW\_below\_th}}$ and $\eta_{\text{inj\_QW\_at\_th}}$. The carrier density in the barrier region (N_B) is related to the N_{QW} from Eq. (10), with the contribution from the S term being neglected in the below-threshold and at-threshold conditions. The at-threshold solution of $\eta_{\text{inj\_QW\_at\_th}}$ is the same as the expression in Eq. (14), only with the expression calculated for the specific case at $N_{\text{QW}} = N_{\text{QW\_th}}$ (threshold carrier density in QW). The expression for $N_{\text{QW\_th}}$ can be extracted from the semilogarithmic expression of the gain versus the carrier density given by $g(N_{\text{QW}}) = g_{oN} \cdot \ln(N_{\text{QW}}/N_{\text{QW\_tr}})$, calculated at threshold for $\Gamma \cdot g(N_{\text{QW\_th}}) = \alpha_i + (1/L)\ln(1/R)$. The value of the $N_{\text{QW\_tr}}$ is the carrier density required in the QW to reach transparency. Typical $N_{\text{QW\_th}}$ values of interest for the 1200 nm emitting InGaAs and the 1300 nm emitting InGaAsN QW lasers range from 2×10^{18} to 4×10^{18} cm^{-3}.

The above-threshold current-injection efficiency of the QW ($\eta_{\text{inj\_QW\_above\_th}}$) is the fraction of the I_{SCH} above threshold that recombines in the QW, after the lasing phenomena occurs. For the above threshold analysis, the expression for the $\eta_{\text{inj\_QW}}$ is very distinct compared to the below threshold conditions. Once the lasing phenomena occurs, the clamping of the modal gain to the total cavity loss will lead to partial or full clamping of the carriers in the QW.[18,23,28] The above-threshold partial-clamping phenomena of carriers in the QW[28] can be a result of carrier heating or a variation in the lateral mode profile. This partial clamping phenomenon typically leads to an unclamping rate of approximately 8%–10% in QW lasers.[23]

To distinguish the threshold and above threshold conditions, the following definitions are made: $I_{\text{SCH\_th}}$ is defined as the total injected current into the SCH region at the threshold condition, and $I_{\text{QW\_th}}$ is defined as the total injected current that recombines in the QW at threshold. The relation of threshold current density (J_{th}) of QW lasers to the $I_{\text{SCH\_th}}$ and $I_{\text{QW\_th}}$ can be expressed as follows:

$$J_{\text{th}} = \frac{I_{\text{SCH\_th}}}{w \cdot L \cdot \eta_{\text{inj\_structure}}} = \frac{I_{\text{QW\_th}}}{w \cdot L \cdot \eta_{\text{inj\_structure}} \cdot \eta_{\text{inj\_QW\_th}}}, \tag{15}$$

with w and L corresponding to the cross-sectional width and length of the devices. The $I_{\text{SCH\_th}}$ can be related to the $I_{\text{QW\_th}}$ $(=N_{\text{QW}} \cdot V_{\text{QW}} / \tau_{\text{QW\_total}})$ by utilizing the relation in Eq. (15) and the expression of the $\eta_{\text{inj\_QW\_th}}$ from Eq. (14).

In realizing the model for $\eta_{\text{inj\_QW\_above\_th}}$, one should revisit Eqs. (9)–(11) again, and apply a differential increase in the I_{SCH} above threshold. The stimulated emission injected current into the SCH region is defined as $I_{\text{SCH\_st}}$ $(=I_{\text{SCH}} - I_{\text{SCH\_th}})$. By allowing the possibility of partial and full clamping of the carriers in the QW, rearranging Eqs. (9) and (10) will result in the expression for $I_{\text{SCH\_st}}$ as follows:

$$\begin{aligned}\frac{I_{\text{SCH\_st}}}{\eta_{\text{inj\_structure}}} &= (J - J_{\text{th}}) \cdot w \cdot L \\ &= \frac{V_{\text{QW}} \cdot \left(1 + \dfrac{\tau_{\text{bw}}}{\tau_b}\right) \cdot q \cdot \left(\dfrac{S/\Gamma}{\tau_p}\right)}{1 - \Delta_{\text{QW}} \cdot \left[\left(1 + \dfrac{\tau_{\text{bw}}}{\tau_b} \cdot \left(1 + \dfrac{\tau_{\text{QW\_total}}}{\tau_e}\right) - \beta \cdot \left(\dfrac{\tau_{\text{bw}}}{\tau_b} + 1\right)\right)\right]},\end{aligned} \tag{16}$$

with Δ_{QW} defined as the relative increase or unclamping rate of the carrier in the QW, which can be expressed as $\Delta_{\text{QW}} = \Delta(N_{\text{QW}} \cdot V_{\text{QW}} / \tau_{\text{QW\_total}}) / \Delta(I_{\text{SCH}}/q)$. For the case of the full clamping of the carriers in the QW, Δ_{QW} will be zero. Since β typically ranges from 0.001 to 0.01, much smaller than unity, the $1/\tau_p$ can be assumed as equal to total cavity loss rate $v_g[\alpha_i + \alpha_m(L)]$.

The total lasing output power of QW lasers (P_{output}) can be expressed as a function of the photon density in the cavity (S), the energy of the photon (E_p), the total photon escape rate ($v_g \cdot \alpha_m$), and the effective volume of the optical mode ($V_{\text{optical}} = V_{\text{QW}}/\Gamma$),[20] with the following relationship:

$$P_{\text{output}} = E_p S \cdot (V_{\text{QW}}/\Gamma) \cdot \nu_g \cdot \alpha_m. \tag{17}$$

From rearranging Eqs. (4), (5), (14), (16), and (17), the above-threshold current injection efficiency ($\eta_{\text{inj\_QW\_above\_th}}$) can be expressed as follows:

$$\eta_{\text{inj\_QW\_above\_th}} = \frac{1 - \Delta_{\text{QW}} \cdot \left(\dfrac{1}{\eta_{\text{inj\_QW\_at\_th}}} - \beta \cdot \left(1 + \dfrac{\tau_{\text{bw}}}{\tau_b}\right)\right)}{1 + \dfrac{\tau_{\text{bw}}}{\tau_b}}, \tag{18}$$

where $\eta_{\text{inj\_QW\_at\_th}}$ depends on the τ_e, τ_{bw}, τ_{QW}, and τ_b. For the case of full clamping of carriers in the QW, the $\eta_{\text{inj\_QW\_above\_th}}$ will reduce to the simple form of $1/(1 + \tau_{\text{bw}}/\tau_b)$. Typical unclamping rates for carriers in the QW (Δ_{QW}) are approximately 8%–12%.[23] The thermionic carrier leakage at high temperature also plays significant role, especially in reducing the $\eta_{\text{inj\_QW\_at\_th}}$ and increasing the $1/\tau_b$, which will in turn lead to a reduction in $\eta_{\text{inj\_QW\_above\_th}}$.

The analysis here shows that the at-threshold and above-threshold current injection efficiency of QW lasers are quite different from one another, explicitly shown in Eqs. (14) and (18). The $\eta_{\text{inj\_QW\_at\_th}}$ will be severely reduced, compared to the $\eta_{\text{inj\_QW\_above\_th}}$, for the case of the QW lasers with large thermionic carrier escape rate $(1/\tau_e)$. Thermionic carrier escape is significant for the QW lasers with poor carrier confinement, reflected by a small ΔE_c or ΔE_v. Only for the case in which the thermionic carrier leakage of a QW laser is negligible $(1/\tau_e \to 0)$ and full clamping occurs for the carriers in QW $(\Delta_{\text{QW}} \to 0)$, are $\eta_{\text{inj\_QW\_at\_th}}$ and $\eta_{\text{inj\_QW\_above\_th}}$ found to be similar.

IV. PARAMETERS OF INTEREST FOR MODELING

A. Parameters of interest

In realizing the current injection efficiency model, we have taken the parameters of interest from various sources. The parameters of interest here include the barrier-QW capture time (τ_{bw}), the thermionic carrier escape time (τ_e), the recombination lifetime in the barriers (τ_b), and in the QW (τ_{QW}). The description of the parameters of interest here is intended to serve as a guideline in modeling and designing the current injection efficiency for any QW lasers in general. The parameters utilized for the case of InGaAs QW and InGaAsN QW lasers will be discussed further in Sec. V.

B. The barrier-well capture time (τ_{bw})

The barrier-well capture time consists of the carrier transport time (τ_r) and the quantum-capture time ($\tau_{\text{cap\_QW}}$).[23,25,27] The $\tau_{\text{cap\_QW}}$ has been neglected in the analysis here due to the dominant contribution from τ_r in the τ_{bw}.[23,25] The $\tau_{\text{cap\_QW}}$ term can be easily included, if necessary, by utilizing $\tau_{\text{bw}} = \tau_r + \tau_{\text{cap\_QW}}$. As a result of very large electric field in the SCH region, the transport of carrier transport from the SCH to the QW follows the ambipolar carrier transport.[25,27] The analytical τ_r for SCH structures with symmetric confinement region,[25,27] with $2 \cdot L_s$ as the total width of the SCH, has been shown to have a rather simple form as follows:

$$\tau_r = \frac{1}{2} \cdot \left(\frac{L_S^2}{2 \cdot D_p} + \frac{L_S^2}{2 \cdot D_n}\right) = \frac{\tau_{r,\text{holes}} + \tau_{r,\text{electrons}}}{2}. \tag{19}$$

The distance L_s is the undoped region of the confinement region, measured from the QW to the edge of the doped-cladding region. For the case in which the confining region is doped, only the undoped confining region should be included in the L_s.[25] For all our lasers modeled here, we utilize the GaAs-confining region. The diffusion coefficient for electrons (D_n) and holes (D_p) can be calculated from the Einstein relation $D_n = (k_B T/q)\mu_n$ and $D_p = (k_B T/q)\mu_p$, with k_B, T, μ_n, μ_p, corresponding to Boltzmann constant, temperature, electron mobility, and hole mobility, respectively. The unintentional background doping of the SCH region will affect the carrier mobility, which will in turn affect the carrier diffusion coefficient. The background doping of metalorganic chemical vapor deposition (MOCVD)-grown undoped GaAs layer is typically slightly n doped, with doping level ranging from low-10^{16} to low-10^{17} cm^{-3} depending on the growth conditions. The majority mobility of electrons and minority mobility of holes in n-GaAs, at $T=300$ K, can be calculated from the following equations:[29,30]

$$\mu_{n\_\text{GaAs\_300 K}} = \frac{7200}{[1+(5.51\times 10^{-17})\cdot N_d]^{0.233}}\ \text{cm}^2/\text{V s}, \tag{20}$$

$$\mu_{p\_\text{GaAs\_300 K}} = \frac{380}{[1+\ 3.17\times 10^{-17})\cdot N_d]^{0.266}}\ \text{cm}^2/\text{V s}, \tag{21}$$

with N_d corresponding to the background doping of the donors in units of cm^{-3}, respectively.

The temperature dependence of the carrier transport time (τ_r) is a result of the temperature dependence of the carrier diffusion coefficient and carrier mobility. For the treatment of the temperature dependence of electron and hole mobility, we follow the expression presented by Sze.[31] The temperature dependence of the electron and hole carrier mobility in GaAs can be expressed as follows:[25,31]

$$\mu_{n\_\text{GaAs}}(T) = \mu_{n\_\text{GaAs\_300 K}}\cdot\left(\frac{300}{T(\text{K})}\right)^{2.1}, \tag{22}$$

$$\mu_{p\_\text{GaAs}}(T) = \mu_{p\_\text{GaAs\_300 K}}\cdot\left(\frac{300}{T(\text{K})}\right)^{2.1}. \tag{23}$$

C. Thermionic carrier escape time (τ_e)

The thermionic carrier lifetime (τ_e) in QW lasers is an important factor in determining the below-threshold, the at-threshold, and the above-threshold current injection efficiency of QW ($\eta_{\text{inj\_QW}}$) lasers, as reflected in Eqs. (13), (14), and (18). A large thermionic lifetime of the carriers in the QW indicates a minimal escape rate of the carriers from the QW to the SCH.[23,25,32–35] Minimal thermionic carrier escape rate out of the QW will lead to an increase in $\eta_{\text{inj\_QW}}$ and a reduction in the temperature sensitivity of $\eta_{\text{inj\_QW}}$. The conventional method to express the thermionic lifetime is based on the model by Schneider *et al.*,[32] which utilizes the bulk three-dimensional (3D) density of states (DOS) and a simple parabolic band model. Unfortunately, this model[32] has been shown to be insufficient to explain experiments,[33] and has a tendency to significantly overestimate the hole lifetime and to underestimate the electron lifetime.[33] The thermionic lifetime model that we employ in this study[34,35] is based on the model proposed by Irikawa *et al.*,[33] that has been applied to study 1500 nm InGa(Al)As/InP QW lasers.

The distinction of the total thermionic carrier leakage with the leakage from QW to one side of SCH is shown in Fig. 2. The derivation of the thermionic current leakage presented here follows the treatment of thermionic emission theory by Bethe[36] and Sze,[31] with the following assumptions: (1) the carriers in the QW are under thermal equilibrium, (2) the net current flow does not affect this equilibrium, and (3) the barrier height is much larger than the thermal energy (k_BT). Under these assumptions, carriers inside the QW will

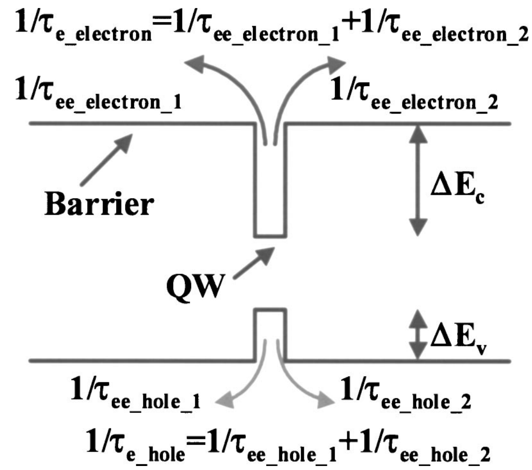

FIG. 2. Schematic of the thermionic carrier leakage processes for QW-active region.

redistribute to maintain the emission of the carriers from the edge of the QW to the barrier region. By utilizing these assumptions, the net thermionic current depends only on the carrier density in the QW (N_{QW}), lattice temperature (T), thickness of QW (L_z), and the barrier height.

The thermionic current leakage, from the edge of a single QW to one side of the SCH, $J_{\text{ee\_}i}$, is related to the thermionic emission carrier lifetime to one side of the SCH $\tau_{\text{ee\_}i}$ as follows:

$$J_{\text{ee\_}i} = NqL_zN_{\text{QW}}/\tau_{\text{ee\_}i}, \tag{24}$$

in which $i, N, q, L_z, N_{\text{QW}}$, represent the type of carriers (electrons or holes), the number of QWs, the charge of the electron, the thickness of QW, and the carrier density in QW, respectively. It is important to note that the thermionic leakage current here is not the same as the total current leakage in QW laser devices, as the leaked carriers into the SCH region will have the probability of being recaptured back and recombine in the QW.[23,25,33–35] The relationships of the total threshold current density and the current injection efficiency with the thermionic carrier lifetime are more complex, and are interrelated by the total recombination lifetime in the QW and barrier regions and carrier capture time into the QW.[23,25,33–35] The thermionic leakage current $J_{\text{ee\_}i}$ has been described in Refs. 29 and 31–35 with the standard thermionic emission theory as follows:

$$J_{\text{ee\_}i} = \frac{4\pi\cdot q\cdot(k_BT)^2}{h^3}\cdot m_i^*\cdot\exp\left(-\frac{E_{\text{b}i}-F_i}{k_BT}\right), \tag{25}$$

where m_i^*, $E_{\text{b}i}$, and F_i are the effective masses of the electrons or holes in the QW, the effective barriers, and the quasi-Fermi levels for the electrons or holes in QW, respectively. The constants k_B and h represent the Boltzmann and Planck constant, respectively. The carrier density in the QW is calculated by taking into consideration the 2D DOS of the strained-QW, strain effects in band gap of the QW, and the Fermi–Dirac statistics.[20] The thermionic escape lifetime ($\tau_{\text{ee\_}i}$) can be extracted by relating the thermionic leakage current ($J_{\text{ee\_}i}$) and the carrier density in the QW (N_{QW}), with appropriate consideration of the structure. The total current leakage from the single quantum well (SQW) to both sides of the SCH, contributed by carrier i (electrons or holes), is $J_{e\_i}=J_{ee\_i\_right}+J_{ee\_i\_left}$. The total thermionic escape lifetime of carrier i (τ_{e_i}) can be expressed as $1/\tau_{e\_i}=1/\tau_{ee\_i\_right}+1/\tau_{ee\_i\_left}$. For the case of symmetrical barriers ($J_{ee\_i\_right}=J_{ee\_i\_left}$), the expression $1/\tau_{e\_i}=2/\tau_{ee\_i}$ will be obtained.

The total thermionic carrier escape time of QW lasers (τ_e) can be expressed as functions of the thermionic escape time of electrons and holes as follows: $1/\tau_e=1/\tau_{e\_electron}+1/\tau_{e\_holes}$. The escape phenomenon is dominated by the escape rate of the carriers with the fastest escape time. Once the carriers have escaped, the carriers in the QW and SCH will redistribute themselves to maintain charge neutrality in QW and SCH attributed to the high mobility of the carriers.[23,25]

D. Recombination in the QW region (τ_{QW})

The recombination of carriers in the QW has been well studied.[19–22] The recombination mechanisms in the QW-active material typically consists of the monomolecular (A), bimolecular (B), and Auger (C) recombination processes with the bimolecular-recombination process leading to optical gain in the material. The radiative recombination rate ($1/\tau_{QW\_rad}$) can be expressed as $1/\tau_{QW\_rad}=B_{QW}N_{QW}$, with B_{QW} defined as the bimolecular recombination coefficient of the QW-active material. The nonradiative recombination rate ($1/\tau_{QW\_non\_rad}$) can be expressed as follows: $1/\tau_{QW\_non\_rad}=A_{QW}+C_{QW}N_{QW}^2$, with A_{QW} and C_{QW} corresponding to the monomolecular- and Auger-recombination coefficient of QW-active material, respectively. The total recombination rate in the QW is then defined as $1/\tau_{QW\_total}=1/\tau_{QW\_rad}+1/\tau_{QW\_non\_rad}$.

E. Recombination in the barrier region (τ_b)

The recombination processes in the barrier/SCH region consist mostly of the monomolecular and bimolecular processes. Typically Auger recombination can be neglected in the analysis for the SCH region, due to the larger band gap of the barrier material and the significantly lower carrier density in the barrier compared to that in the QW region. The τ_b can then be expressed as $1/\tau_b=A_B+B_BN_B$, with A_B and B_B corresponding to the monomolecular- and bimolecular-recombination coefficient of barrier/SCH material, respectively. The carrier density in the SCH region (N_B) is related to the carrier density in the QW (N_{QW}), from Eq. (10). For analysis of the near-threshold condition, the photon density (S) can be assumed to be zero. As the thermionic carrier escape rate increases ($1/\tau_e$), the overflow of the carrier in the SCH region will be significant, which will in turn lead to an increase in the recombination current in the SCH region ($I_B=N_BV_B/\tau_b$).

V. THERMIONIC CARRIER ESCAPE TIMES FOR THE InGaAs(N) QW

In this study,[34] the τ_{ee_i} values are analyzed for the case of the 1190 nm emitting InGaAs QW and 1300 nm emitting InGaAsN QW lasers. These 1190–1300 nm InGaAs(N) QW lasers, shown schematically in Fig. 3, are similar to the lasers that we have published previously,[4,5] in which a very high In content (~40%) and minimum N content (~0.5%) InGaAs(N) QW is utilized to achieve high performance λ=1190–1300 nm emitting lasers with GaAs as the direct barrier to the QW. Large band-gap $Al_{0.74}Ga_{0.26}As$ layers are utilized as the n- and p-cladding layers, to ensure minimal carrier leakage from the SCH region to cladding layers.

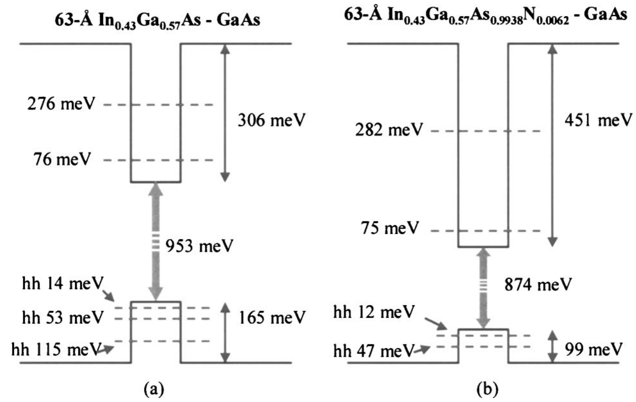

FIG. 3. Band lineup for conduction and valence bands of: (a) 1190 nm $In_{0.43}Ga_{0.57}As$ QW and (b) 1295 nm $In_{0.43}Ga_{0.57}As_{0.9938}N_{0.0062}$ QW lasers, with GaAs barriers.

The existence of the small N content (~0.5–2%) in the InGaAsN QW mainly affects the conduction band, which allows for the approximation of many of the material parameters of the $In_xGa_{1-x}As_{1-y}N_y$ QW with those of the $In_xGa_{1-x}As$ QW.[37] The compilation of the parameters used here follows the treatment in Refs. 37 and 38 for the effective masses of the electrons, band-gap energy, and conduction (ΔE_c) and valence (ΔE_v) band offsets.

We determine the appropriate band-offset values by fitting the theory with the measured values from the experiments. The conduction-band-offset ratio ($Q_c=\Delta E_c/\Delta E_g$) for highly strained (In>20%) InGaAs–GaAs materials has been predicted to be in the range 60%–65%.[20,21,39–42] For the case of the InGaAsN QW, experimental studies[3,38] show that Q_c is as high as 77%–80% for the case of $In_{0.38}Ga_{0.62}As_{0.985}N_{0.015}$. Additional recent work[43] has also demonstrated experimentally the reduction in the valence band offset (ΔE_v) in InGaAsN QW as a result of N incorporation into InGaAs QW. We found very good agreement in emission wavelength and QW composition between theory and experiment with Q_c values of 65%, and 82% for 63 Å $In_{0.43}Ga_{0.57}As$ QW, and 63 Å $In_{0.43}Ga_{0.57}As_{0.9938}N_{0.0062}$ QW, respectively. The compositions, the QW thickness, and the emission wavelengths of both the 60 Å $In_{0.4}Ga_{0.6}As$ QW and 60 Å $In_{0.4}Ga_{0.6}As_{0.995}N_{0.005}$ QW are measured experimentally.[2,5] The m_e^* for InGaAs QW and InGaAsN QW here are calculated as $0.047m_0$ and $0.069m_0$, respectively, with m_0 as mass of electron. The m_{hh}^* for both InGaAs and InGaAsN QW utilized in calculation is $0.457m_0$. Due to the large strain of the InGaAs and InGaAsN QW, the hole band structure consists of only heavy-hole (hh) subbands in the 2D states, with light-hole (lh) states having bulk-like (3D) properties. As shown in Table I, we found there exists very good agreement between the theory and experiments with Q_c values of approximately 65%, and 82% for $In_{0.4}Ga_{0.6}As$ QW, and $In_{0.43}Ga_{0.57}As_{0.9938}N_{0.0062}$ QW, respectively.

TABLE I. Parameters of InGaAs-QW and InGaAsN-QW laser structures.

InGaAs(N) QW	t_{QW} (Å)	In (%)	N (%)	λ (μm)	$\Delta E_c/\Delta E_v$
Experiments[a]	60	40	0	1.185	—
	60	40	0.5	1.295	—
Theory	63	43	0	1.19	0.65/0.35
	63	43	0.62	1.295	0.82/0.18

[a]See Ref. 1.

By utilizing the parameters listed in Refs. 33–42 and Fig. 3, the thermionic escape lifetime τ_{ee_i} can be calculated for electrons and holes for both InGaAs and InGaAsN QWs, as shown in Fig. 4. For the case of an InGaAs QW, the τ_{ee} (~50–160 ps) of electrons is comparable to that (~55–60 ps) of heavy holes, for typical threshold carrier density of interest ($N_{QW} \sim 1.5–4 \times 10^{18}$ cm^{-3}). In the case of an InGaAsN QW, the τ_{ee} of the heavy hole is significantly smaller than τ_{ee} of the electron. The electrons are very well confined in the InGaAsN QW, as indicated by the large τ_{ee} (~40–100 ns) of the electron for typical threshold conditions. This large τ_{ee} of electrons in InGaAsN QW is expected, owing to its large conduction band offset (ΔE_c ~450 meV). On the other hand, the heavy hole is very poorly confined due to the large disparity of the ΔE_c and ΔE_v. The small valence band offset (ΔE_c~99 meV) in InGaAsN QW results in a picosecond range τ_{ee} of approximately 5–6 ps, for typical threshold conditions. Due to the significantly smaller τ_{ee} of the hole in the InGaAsN QW, the heavy-hole leakage is the dominant leakage mechanism for the InGaAsN QW. Severe thermionic carrier leakage leads to a reduction in the current injection efficiency at threshold,[23,25,35] which is distinct from the above-threshold η_{inj},[18] and will in turn lead to an increase in the threshold current density of the QW laser.

The thermionic carrier escape lifetimes for the InGaAs and InGaAsN QWs are shown in Figs. 5(a) and 5(b), respectively. At elevated temperature (T=360 K), τ_{ee} of the heavy hole reduces to only 3 ps, as shown in Figs. 5(b) and 6. In the case of the InGaAs QW, the lowest τ_{ee} is approximately 21 ps at an elevated temperature of 360 K. The severe heavy-hole leakage at elevated temperature for InGaAsN QW lasers serves as one of the contributing factors that leads to the highly temperature sensitive (T_0~70–90 K) threshold current of high-performance 1300 nm InGaAsN QW lasers. Although the hole-leakage processes may dominate the high temperature sensitivity of InGaAsN QW lasers, Auger recombination and other processes in the InGaAsN QW cannot be ruled out as contributing factors.

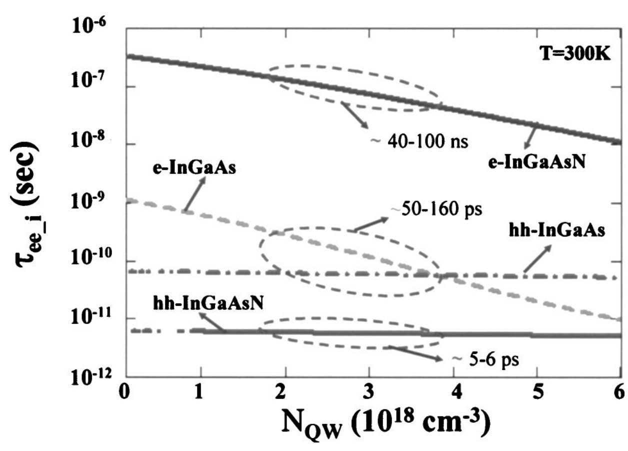

FIG. 4. The electron and hole thermionic escape lifetimes of 1190 nm InGaAs QW and 1295 nm InGaAsN QW lasers with GaAs barriers, at T =300 K, as a function of N_{QW}.

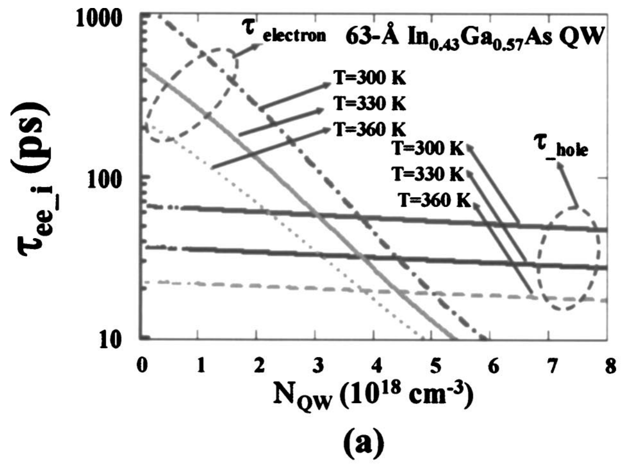

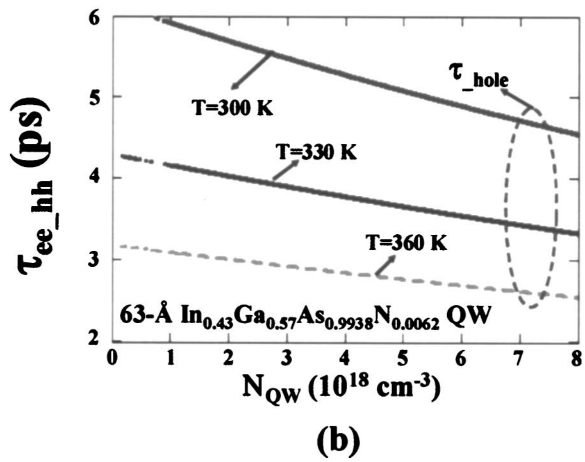

FIG. 5. The electron and hole thermionic escape time of the: (a) 1190 nm InGaAs QW and (b) 1295 nm InGaAsN QW lasers with GaAs barriers, as functions of N_{QW} and temperature.

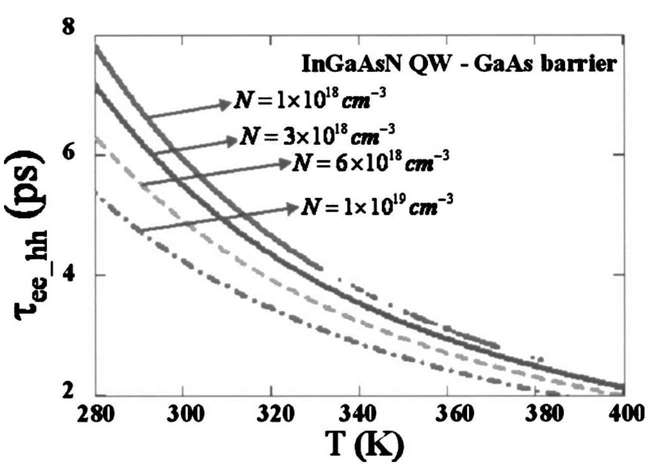

FIG. 6. The τ_{ee_hh} of 1295 nm InGaAsN QW with various N_{QW}, as a function of temperature.

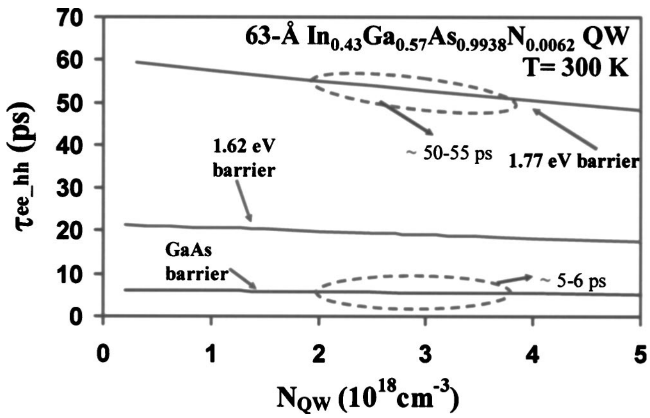

FIG. 7. The τ_{ee_hh} of InGaAsN QW with various barriers at T=300 K, as a function of N_{QW}.

To achieve suppression of hole leakage from the InGaAsN SQW, larger band-gap materials of tensile GaAsP or InGaAsP can also be utilized as the direct barrier or SCH regions. As shown in Fig. 7, the τ_{ee} of holes (τ_{ee_hh}) in an InGaAsN QW are calculated for structures with various barrier regions. By utilizing the 1.77 eV InGaAsP lattice-matched barriers, with the assumption of a band-offset ratio ($\Delta E_c:\Delta E_v$) of 82:18, the thermionic escape rate ($1/\tau_{ee\_holes}$) of the heavy hole in InGaAsN QW is reduced significantly by approximately 10–12 times, in comparison with that of the InGaAsN–GaAs case. In fact, the τ_{ee_holes} ($\sim$25 ps, N_{QW} $\sim 3\times 10^{18}$ cm^{-3}, T=360 K) of the heavy hole for an InGaAsN QW with 1.77 eV barriers at elevated temperature, is comparable with the lowest τ_{ee} of carriers in an InGaAs QW for typical threshold conditions at the same temperature. The utilization of an InGaAsN multiple QW with GaAs barriers is also expected to improve the high-temperature laser performance. The utilization of a multiple QW active region will result in a lower thermionic hole escape rate ($1/\tau_{ee\_holes}$), as the $1/\tau_{ee}$ is inversely proportional to the number of QWs (N), indicated from Eq. (24).

The hole-leakage process is identified as the main mechanism in the leakage process in 63 Å $In_{0.43}Ga_{0.57}As_{0.9938}N_{0.0062}$ SQW lasers with GaAs barriers. At a typical room-temperature threshold carrier density (N_{QW} $=1.5-3\times 10^{18}$ cm^{-3}), the estimated τ_{ee} for the hh in 1300 nm emitting InGaAsN QW lasers is predicted to be around 5–6 ps, which is approximately ten times smaller than that of the 1190 nm emitting InGaAs QW lasers. Reduction in the hole leakage, by utilizing large-band gap barriers in a SQW, should allow the realization of high-lasing performance and high-temperature operation 1300 nm InGaAsN SQW lasers, comparable to that achieved with 1190 nm emitting InGaAs SQW lasers. Utilization of multi-QW InGaAsN active regions will also allow reduction in the thermionic carrier escape rate, which will be beneficial for high-temperature operation.

The intent of the analysis presented in this section is to point out the significance of the thermionic carrier escape processes in 1300 nm InGaAsN QW lasers, which have been neglected in previous analysis under the assumption of strong electron confinement.[17] The role and impact of the significant hole leakage in InGaAsN QW on the current injection efficiency of InGaAsN QW lasers will be discussed in detail in Sec. VI.

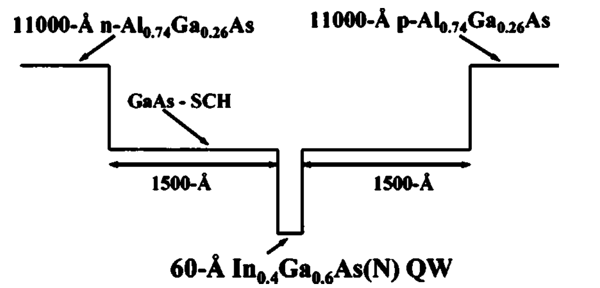

FIG. 8. Schematic of the InGaAs(N) QW laser structures, simulated here.

VI. CURRENT INJECTION EFFICIENCY OF InGaAs(N) QW-SIMULATION

A. Design of experiments and structures

The structures that we utilize in these simulations are based on the laser structures that have been fabricated and studied experimentally.[4] The laser structure is shown in Fig. 8, consisting of 60 Å QW of either a 1200 nm $In_{0.43}Ga_{0.57}As$ QW or a 1300 nm $In_{0.43}Ga_{0.57}As_{0.9938}N_{0.0062}$ QW active region. The compositions of the QWs studied here are similar to the QW compositions of the laser structures studied experimentally.[4] For simplicity and without loss of generality, the analysis will be primarily focused on the case for structures utilizing a single QW. The QW active region is sandwiched inside a 3000 Å undoped GaAs optical confinement layer, which is also similar to our typical 1200 nm InGaAs QW and 1300 nm InGaAsN QW laser structures.[3,4] The assumption of minimal carrier leakage from the confinement layer out into the cladding layers is valid, due to the utilization of the large band gap material of $Al_{0.74}Ga_{0.26}As$ as the cladding layers.

The parameters utilized in the calculation of the current injection efficiencies follow the treatment presented in Sec. IV and V. The optical confinement layer of undoped GaAs is assumed to have slightly n-type background doping of 10^{16} cm^{-3}, which is typical for undoped GaAs grown by MOCVD at low temperature. From Eqs. (19)–(23), the carrier transport time (τ_r) and the barrier capture time (τ_{bw}) can be extracted. Thermionic carrier escape lifetimes utilized here for both InGaAs and InGaAsN QWs active regions with GaAs barrier regions have been calculated and discussed in Sec. V.

The carrier recombination in the undoped-GaAs SCH region consists of both the monomolecular and bimolecular processes. The Auger recombination process is assumed to be minimal in an undoped GaAs material system, which is utilized for the optical confinement layer. Lower carrier density in the SCH region, in comparison to that of QW (N_{QW}), also validates the assumption of minimal Auger recombination processes in the SCH region. The recombination rate in the SCH region ($1/\tau_b$) is calculated from $1/\tau_b = A_B + B_B N_B$, where A_B and B_B terms are assumed as approximately 1×10^8 s^{-1} and 1.2×10^{-10} cm^3/s, respectively, which are typical for the GaAs material system.[21]

The carrier recombination in the 1200 nm InGaAs QW and the 1300 nm InGaAsN QW active regions consist of monomolecular, bimolecular, and Auger processes. Theoretical gain calculations have shown that the incorporation of N into an InGaAsN QW only results in a reduction of approximately 10% of its peak optical gain, in comparison to the N-free InGaAs QW.[44] Here we assume the bimolecular recombination rate for both the InGaAs and InGaAsN QW as identical to B_{QW} of 1.5×10^{-10} cm^3/s, which is a typical value for InGaAs QW.[21] For the analysis of optimized, high-performance 1300 nm emitting InGaAsN QW and 1200 nm emitting InGaAs QW lasers, the monomolecular recombination rate of these two active regions can be assumed to be minimal and identical. It is very important to emphasize that the assumption of the minimal monomolecular recombination process in the InGaAsN QW active region is valid only for the analysis of the highest-performance InGaAsN QW laser (many of the earlier reported InGaAsN lasers exhibited very high monomolecular recombination rates). Here we only consider optimized and very low J_{th} 1200 nm emitting InGaAs QW and 1300 nm emitting InGaAsN QW lasers.[3,4] The monomolecular recombination rate for both the InGaAs QW and InGaAsN QW is assumed to be identical with A_{QW} of 1×10^8 s^{-1}. Variation of the monomolecular recombination rate (A_{QW}) of the 1300 nm InGaAsN QW lasers will also be studied to understand the role of nonradiative recombination on its current injection efficiency. The role of Auger recombination in InGaAsN lasers is still very controversial. While Auger recombination has been implicated[2] in the temperature sensitivity of InGaAsN lasers, these studies have not necessarily been conclusive in demonstrating the extent of the Auger recombination process in high-performance 1300 nm InGaAsN QW lasers. Studies without taking into account any carrier leakage,[2] may have significantly overestimated the Auger rate in the presence of a large thermionic carrier leakage in the 1300 nm InGaAsN QW lasers.[16,17] Here we assume that the Auger recombination rate for both the 1200 nm InGaAs QW and the 1300 nm InGaAsN QW as similar to C_{QW} of 5×10^{-30} cm^6/s, which is a typical value for InGaAs QW.[21] We found that, even in the presence of minimal Auger recombination in the 1300 nm InGaAsN QW laser, the thermionic heavy hole leakage process may significantly contribute to a large increase in the threshold current density and temperature sensitivity at elevated temperatures.

B. The below- and at-threshold conditions

The at-threshold current-injection efficiency of the QW ($\eta_{inj\_QW\_at\_th}$) for both the 1200 nm emitting InGaAs QW and 1300 nm emitting InGaAsN QW lasers are calculated as a function of temperature, and shown in Fig. 9. The $\eta_{inj\_QW\_at\_th}$ is calculated from Eq. (14), utilizing the parameters presented in Sec. IV, V, and VI A. The typical threshold carrier density in the QW (N_{QW_th}) for QW lasers is in the range of 2.5×10^{18}–4×10^{18} cm^{-3}. Here we assume N_{QW_th} of 3×10^{18} cm^{-3} for both the InGaAs QW and InGaAsN QW lasers at a temperature of 300 K. In these studies, we are interested primarily in the temperature evolution of the $\eta_{inj\_QW\_at\_th}$ (not their absolute values) for both InGaAs and InGaAsN QW lasers. The temperature dependence of the N_{QW_th} can be approximated, in a limited temperature regime, to follow a linear relation with temperature (T).[22]

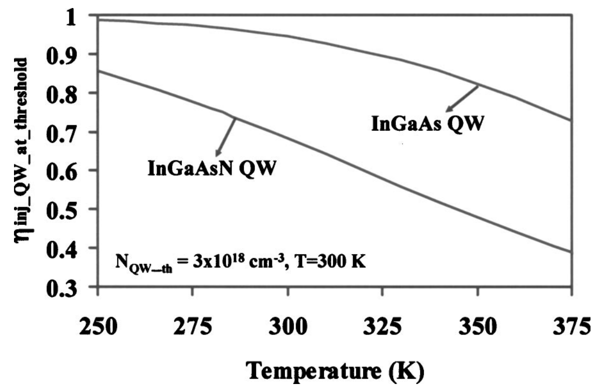

FIG. 9. The $\eta_{inj\_QW\_at\_th}$ for InGaAs and InGaAsN QW lasers, as a function of temperature.

The $\eta_{inj\_QW\_at\_th}$ value for a QW laser is very important, as it will determine the fraction of the injected threshold current density that actually recombines in the QW. A severe reduction in the $\eta_{inj\_QW\_at\_th}$ of QW lasers will result in a significant increase in the total injected current density required to reach threshold. From the calculation presented in Fig. 9, the $\eta_{inj\_QW\_at\_th}$ of InGaAsN QW lasers is only approximately 65% at T=300 K, which is very distinct from that ($\eta_{inj\_QW\_at\_th}$=95%) of InGaAs QW lasers. The low $\eta_{inj\_QW\_at\_th}$ of 1300 nm emitting InGaAsN QW lasers may partially explain the larger (observed) room-temperature J_{th}, in comparison to that of 1200 nm emitting InGaAs QW lasers. $\eta_{inj\_QW\_at\_th}$ values of only 35%–40% are calculated for InGaAsN QW lasers in the temperature regime of 370–380 K, which will lead to a significant increase in the J_{th} at elevated temperatures. In contrast to the case for InGaAsN QW lasers, the $\eta_{inj\_QW\_at\_th}$ of InGaAs QW lasers is very high at room temperature and elevated temperature. The calculated $\eta_{inj\_QW\_at\_th}$ for the InGaAs QW lasers are in excess of 95% and 73% at temperatures of 300 and 370 K, respectively.

From our studies, we found that the contribution of carrier leakage in InGaAsN QW lasers can easily account for almost a factor of 2.2 times increase (120% increase) in the J_{th} at elevated temperature (T=400 K), in comparison to that of room temperature (T=300 K). For the case of InGaAs QW lasers, the carrier leakage effect results only in a factor of 1.5 times increase (50% increase) in the J_{th} at T=400 K, in comparison to that of room-temperature J_{th}.

C. The above-threshold condition

The above-threshold current-injection efficiency of the QW ($\eta_{inj\_QW\_above\_th}$) for both the 1200 nm emitting InGaAs QW and 1300 nm emitting InGaAsN QW lasers are calculated as a function of temperature, and shown in Fig. 10. The $\eta_{inj\_QW\_above\_th}$ is calculated from Eq. (18), utilizing the parameters presented in Secs. IV, V, and VI A. The unclamping

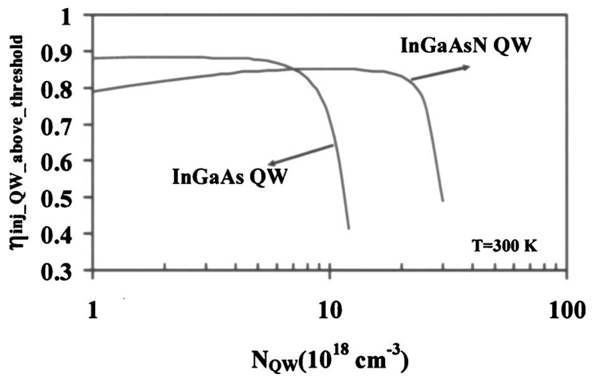

FIG. 10. The $\eta_{\text{inj\_QW\_above\_th}}$ for InGaAs and InGaAsN QW lasers, as a function of N_{QW}.

rate of carriers in the QW (Δ_{QW}) for both InGaAs QW and InGaAsN QW lasers is assumed to be identical to Δ_{QW} of 11%, which is a typical value for QW lasers in general.[23]

From the calculation shown in Fig. 10, we do not observe much dependence of the $\eta_{\text{inj\_QW\_above\_th}}$ with carrier density in the QW (N_{QW}) for both InGaAs QW and InGaAsN QW lasers at room temperature ($T=300$ K) and typical threshold carrier density ($N_{\text{QW\_th}}$). Typical $N_{\text{QW\_th}}$ for QW lasers range from 2.5×10^{18} to 4×10^{18} cm^{-3}. Up to N_{QW} of 10^{19} cm^{-3}, high $\eta_{\text{inj\_QW\_above\_th}}$ can be achieved for both the InGaAs QW and InGaAsN QW lasers for room temperature operation. From the calculated results here, it is evident that the $\eta_{\text{inj\_QW\_above\_th}}$ can be very distinct in comparison to the $\eta_{\text{inj\_QW\_at\_th}}$. The $\eta_{\text{inj\_QW\_at\_th}}$ and $\eta_{\text{inj\_QW\_above\_th}}$ of the 1300 nm InGaAsN QW lasers are calculated as 65% and 85%, respectively, for the case of $N_{\text{QW\_th}}$ of 3×10^{18} cm^{-3} at $T=300$ K. Only in the case of minimal carrier leakage (i.e., 1200 nm emitting InGaAs QW lasers) can the $\eta_{\text{inj\_QW\_above\_th}}$ and $\eta_{\text{inj\_QW\_at\_th}}$ be approximated as similar.

The above-threshold current-injection efficiencies ($\eta_{\text{inj\_above\_th}}$, with $\eta_{\text{inj\_above\_th}}=\eta_{\text{inj\_structure}}\times\eta_{\text{inj\_QW\_above\_th}}$) as a function of temperature for both the 1200 nm InGaAs QW and 1300 nm InGaAsN QW lasers are calculated and compared with experiments, as shown in Fig. 11. It is important to note that the $\eta_{\text{inj\_above\_th}}$ is different from the $\eta_{\text{inj\_QW\_above\_th}}$ by a factor of $\eta_{\text{inj\_structure}}$, as shown in Eq. (2). The experimentally measured quantity, from the plot of $1/\eta_d$ versus L, will result in $\eta_{\text{inj\_above\_th}}$. The experimental data

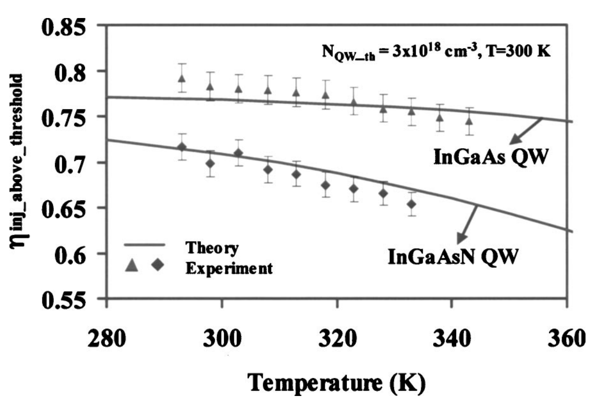

FIG. 11. The $\eta_{\text{inj\_above\_th}}$ for InGaAs and InGaAsN lasers, as a function of temperature.

were taken from the InGaAs QW and InGaAsN QW lasers that utilize a similar SCH region,[1,3] with tensile-strained InGaP–GaAsP buffer layers. These lasers have been discussed in detail in Refs. 1 and 3. The defect-induced carrier recombination at the poor interface of the *n*-AlGaAs cladding layer and the InGaP buffer layer in these laser structures has led to a reduction of the $\eta_{\text{inj\_structure}}$ value. Improvement in the $\eta_{\text{inj\_above\_th}}$, by removing the poor interface of AlGaAs–InGaP, has also been demonstrated to result in improvement of $\eta_{\text{inj\_above\_th}}$.[4]

By taking into account the appropriate $\eta_{\text{inj\_structure}}$ of 88% and 85% for the InGaAs QW and InGaAsN QW lasers, excellent agreement between experiments and theory are observed and shown in Fig. 11. Both the $\eta_{\text{inj\_above\_th}}$ and $\eta_{\text{inj\_QW\_above\_th}}$ of the 1300 nm InGaAsN QW lasers are calculated and experimentally measured to have higher temperature sensitivity, in comparison to those of 1200 nm InGaAs QW lasers. The InGaAs QW lasers exhibit minimal reduction in efficiency up to elevated temperatures of 350 K. In contrast to that of InGaAs QW lasers, the $\eta_{\text{inj\_above\_th}}$ of InGaAsN QW lasers reduces from 72% at $T=293$ K to 65% at $T=333$ K. Aside from the reduction of the $\eta_{\text{inj\_QW\_at\_th}}$, thermionic carrier leakage also leads to a severe reduction in the $\eta_{\text{inj\_QW\_above\_th}}$. It is clear from the experimental and theoretical studies presented in Fig. 11, that heavy-hole leakage in 1300 nm InGaAsN QW lasers can explain the more temperature-sensitive $\eta_{\text{inj\_above\_th}}$, in comparison to that observed in the 1200 nm InGaAs QW lasers.

D. The role of nonradiative recombination

The current injection efficiency of a QW laser depends significantly on the rate of the nonradiative processes. There has been a common misunderstanding or misinterpretation in the literature on the role of nonradiative recombination on the current injection efficiency of QW lasers.[12] Common understanding typically attributes the reduction in the current injection efficiency of InGaAsN QW lasers to the result of an increase in the defect recombination in the QW.[12] From our studies here, we show that the current injection efficiency of QW lasers actually increases as the defect recombination rate increases. The phenomena of increasing current injection efficiency with increasing defect recombination in the QW can be explained by the faster recombination rate of the carriers in the QW when large nonradiative recombination is present.

The common misunderstanding in the role of defects on the current injection efficiency is a result of a misconception of the internal efficiency and current injection efficiency. The current injection efficiency, extracted above threshold, is not the same as internal efficiency. As shown in Eq. (1), the internal efficiency is composed of both the current injection efficiency and the quantum efficiency ($\eta_{\text{Quantum\_Efficiency}}=R_{\text{rad}}/R_{\text{total}}$). The $\eta_{\text{inj\_above\_th}}$ is the differential fraction of the injected current that recombines in the QW, after the lasing phenomena occurs. From multiple-length studies on lasers, plotting the inverse of the above-threshold external differential quantum efficiency ($1/\eta_d$) versus cavity length (L_{cav}), only the $\eta_{\text{inj\_above\_th}}$ can be extracted as described in Sec. II C and Eq. (5).

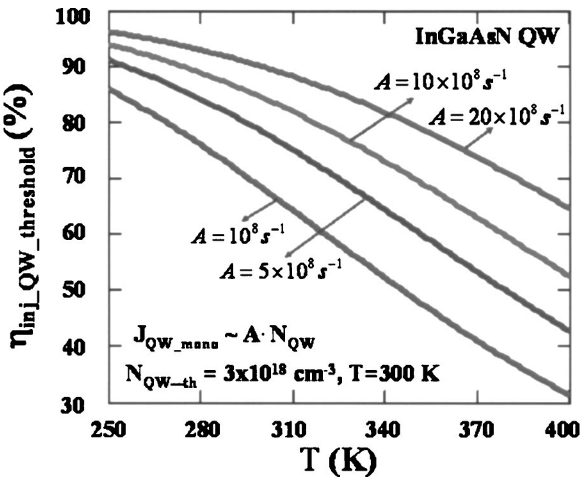

FIG. 12. The $\eta_{\text{inj\_QW\_at\_th}}$ for 1300 nm InGaAsN lasers, as functions of T and A rates.

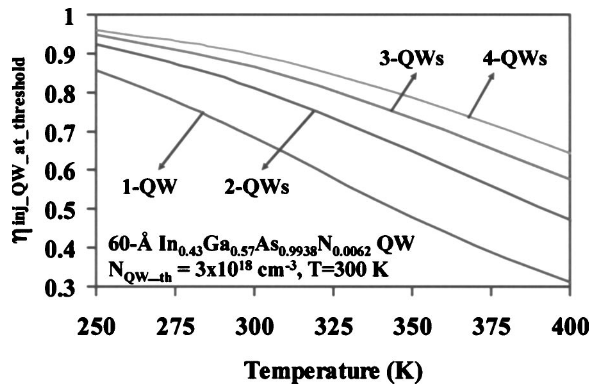

FIG. 13. The $\eta_{\text{inj\_QW\_at\_th}}$ for InGaAsN multiple-QW lasers, as a function of temperature.

The calculated at-threshold current injection efficiency ($\eta_{\text{inj\_QW\_at\_th}}$) of the 1300 nm InGaAsN QW lasers as a function of temperature and defect recombination rate (A) is shown in Fig. 12. As the defect recombination rate (A) increases, the carrier recombination lifetime in the QW (τ_{QW}) will be reduced. A reduction in the τ_{QW} will lead to an increase in the recombination current in the QW. Carriers in the QW can either recombine in the QW through radiative or nonradiative recombination, or be leaked out from the QW through thermionic carrier leakage. An increase in the nonradiative recombination processes in the QW will only lead to an increase in the recombination current in the QW, which in turn leads to an increase in the current injection efficiency. From the calculation results shown in Fig. 12, $\eta_{\text{inj\_QW\_at\_th}}$ of the InGaAsN QW, with increasing defect recombination rate, exhibits a reduction in its temperature sensitivity. The $\eta_{\text{inj\_QW\_at\_th}}$ of the QW with a low defect density ($1\times10^8\ \text{s}^{-1}$) has a value of only approximately 30% at $T=400$ K. By contrast, the $\eta_{\text{inj\_QW\_at\_th}}$ of the QW with a large defect density ($10–20\times10^8\ \text{s}^{-1}$) exhibits a reduction in the temperature sensitivity, which leads to a $\eta_{\text{inj\_QW\_at\_th}}$ of approximately 55%–65% at $T=400$ K.

E. Multiple-QW structures

The poor at-threshold current-injection efficiency of the QW ($\eta_{\text{inj\_QW\_at\_th}}$) in 1300 nm InGaAsN lasers is attributed to the poor confinement of the heavy holes inside the QW. One of the methods that can be utilized to improve the $\eta_{\text{inj\_QW\_at\_th}}$ of 1300 nm InGaAsN QW lasers is by utilizing the multiple QW structures. Utilizing the multiple QW structures will allow for a reduction of the effective thermionic carrier escape rate. The thermionic carrier escape rate ($1/\tau_e$) can be calculated from Eq. (24), where N represents the number of QWs.

It is important to note that Eq. (24) is valid for multiple QW structures, with the assumption that the tunneling rate and the recombination rate in the barrier regions separating QWs are minimal. Carrier tunneling rate across the barrier region can be significant, if the distance between QWs is thin enough. In all our designs and experiments, the distance between QWs is typically in excess of 75–100 Å, which in turn leads to a negligible carrier tunneling processes. Recombination in the barrier regions separating QWs can be neglected as the typical separation of these barrier regions is only on the order of 75–100 Å each. An additional benefit from the utilization of multiple quantum well structures is the lower threshold carrier density in the QW ($N_{\text{QW\_th}}$) in each QW, which is a result of the reduction in the required gain per QW.

From Eq. (24) within the boundary of the assumptions explained earlier, one can approximate the thermionic carrier escape lifetime (τ_e) to scale inversely proportional to the number of QWs (N). By utilizing Eq. (24) and the parameters listed in Sec. IV, V, and VI A, the $\eta_{\text{inj\_QW\_at\_th}}$ as a function of temperature is calculated for the cases of single QW and multiple QWs, and shown in Fig. 13, where the utilization of multiple-QW structures leads to an increase in $\eta_{\text{inj\_QW\_at\_th}}$, in comparison to that of a single-QW structure. Single-QW structures exhibits low $\eta_{\text{inj\_QW\_at\_th}}$ values of only 31% at $T=400$ K. In contrast to the case for a single-QW structure, the $\eta_{\text{inj\_QW\_at\_th}}$ of multiple-QW structures with three and four QWs exhibit reasonably high values of approximately 58% and 65%, respectively, at $T=400$ K. The suppression of heavy-hole leakage in the multiple-QW structure will lead to a reduction in the temperature sensitivity of the J_{th}.

F. Larger-band gap barriers

The thermionic carrier leakage of QW lasers can be suppressed by implementing larger band gap barrier materials to surround the QW. As shown in Sec. V and Refs. 16 and 34, the thermionic escape lifetime of the holes in the InGaAsN QW can be significantly increased by utilizing the large band gap material in the barriers.

Here we calculate the impact of utilizing a larger band gap barrier material on the at-threshold current injection efficiency of QW ($\eta_{\text{inj\_QW\_at\_threshold}}$) of a InGaAsN single-QW laser, as shown in Fig. 14. The calculations here are conducted with GaAs, 1.62 eV InGaAsP, and 1.77 eV InGaAsP barrier materials. The thermionic carrier escape times for all the choices of barrier materials here have been discussed in detail in Sec. V and Refs. 16 and 34.

The utilization of larger band gap materials of 1.52 or 1.62 eV InGaAsP barriers surrounding InGaAsN single-QW

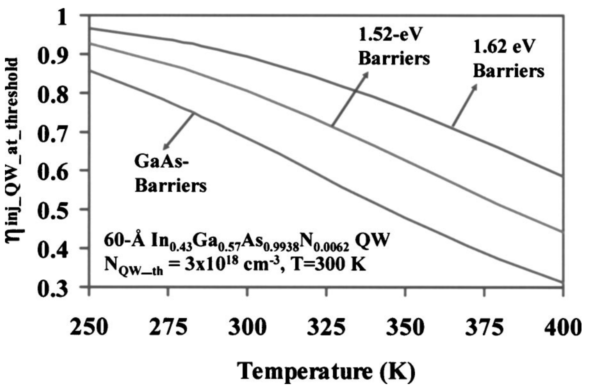

FIG. 14. The $\eta_{inj\_QW\_at\_th}$ for InGaAsN QW lasers with various barriers, as a function of T.

results in a significant increase of the $\eta_{inj\_QW\_at\_th}$ value, as shown in Fig. 14. The InGaAsN QW with GaAs barriers exhibits a low $\eta_{inj\_QW\_at\_th}$ value of only approximately 31% at $T=400$ K. In contrast to the case for a QW structure with GaAs barriers, the $\eta_{inj\_QW\_at\_th}$ of the QW structures utilizing larger band gap barriers of 1.52 and 1.62 eV are calculated as approximately 45% and 60%, respectively, at $T=400$ K. The reduced temperature sensitivity in $\eta_{inj\_QW\_at\_th}$ of the InGaAsN QW structures utilizing larger band gap barrier materials is a result of suppression of thermionic carrier leakage. Suppression of carrier leakage in InGaAsN QW laser, with larger band gap barrier materials, will potentially result in reduced threshold-current density at elevated temperature.

VII. IMPACT OF CARRIER LEAKAGE EFFECT ON LASING CHARACTERISTICS

A. Threshold current density

The existence of large carrier leakage in a QW laser will significantly impact the temperature characteristic of its threshold current density. Carrier leakage is often neglected in the analysis of temperature sensitivity of threshold current density of QW lasers,[2,20,45,46] many times this stems from the misunderstanding of the concept of $\eta_{inj\_QW\_at\_th}$ and $\eta_{inj\_QW\_above\_th}$.

As shown in Fig. 15, we calculate the fractional contribution of the carrier leakage effect on the J_{th} for both the 1200 nm InGaAs and 1300 nm InGaAsN QW lasers as a function of temperature. The fractional contribution of the carrier leakage effect on J_{th} is calculated with respect to the calculated J_{th} at temperature of 250 K. The fractional contribution of the carrier leakage follows the relation $\Delta J_{th\_carrier\_leakage}(T)/J_{th}(T=250\text{ K})$, with $\Delta J_{th\_carrier\_leakage}(T)$ is defined as $J_{th}(T=250\text{ K})/\eta_{inj\_QW\_at\_th}(T)$. As shown in Fig. 15, the carrier leakage effect in 1300 nm InGaAsN QW lasers contributes to a significant increase in the threshold current, up by 120% and 180% at temperatures of 370 and 400 K, respectively. By contrast, the carrier leakage effect only contributes to an approximately 30% increase in the threshold current of the 1200 nm InGaAs QW lasers at a temperature of 370 K.

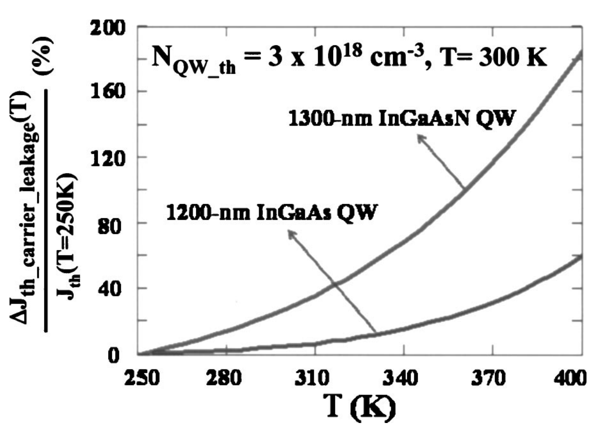

FIG. 15. Fractional contribution of carrier leakage effect on the J_{th} for InGaAs and InGaAsN QW lasers, normalized to $J_{th}(T=250\text{ K})$, as a function of temperature.

It is important to note that carrier leakage in QW lasers is only one part of several contributing factors affecting the temperature sensitivity of the threshold current density. Carrier leakage is often neglected in the analysis of the temperature sensitivity of the threshold current density of QW lasers.[2,20,45,46] The wrong utilization of $\eta_{inj\_above\_th}$ in a threshold analysis in QW lasers, instead of $\eta_{inj\_at\_th}$ as shown in Eq. (3), may also lead to a significant overestimation of the recombination current in the QW. These wrong assumptions can lead to wrong interpretations of results. Neglecting the carrier leakage effect in QW lasers may also lead to a significant overestimation of the Auger recombination rates in the QW, as well as overestimating the temperature sensitivity of the material gain parameter and the internal loss of QW lasers.

The material gain parameter in a QW laser, which suffers from severe carrier leakage, may also be significantly underestimated. The conventional gain parameter utilized in modeling optical gain g_{oJ} follows a semilogarithmic relation as $g_{th}=g_{oJ}\ln(\eta_{inj\_at\_th}J_{th}/J_{tr})$. The term $\eta_{inj\_at\_th}J_{th}$ represents the fraction of the total injected current that actually recombines in the QW, at the threshold condition. Neglecting the carrier leakage effect in QW lasers, with severe carrier leakage, may potentially lead to a significant underestimation of the g_{oJ} value. This underestimation of g_{oJ} can result from an analysis that does not take into account the fact that the total recombination current in the QW is not equal to the total injected current.

B. External differential quantum efficiency

As shown above, thermionic carrier leakage in QW lasers will affect both the at-threshold and above-threshold current injection efficiency. The external differential quantum efficiency (η_d) of a QW laser is linearly proportional to its above-threshold current injection efficiency ($\eta_{inj\_QW\_above\_th}$), as shown in Eq. (5). By suppressing the thermionic carrier leakage out of the QW, a reduction in the temperature sensitivity of the $\eta_{inj\_QW\_above\_th}$ will result in a temperature-insensitive external differential quantum efficiency.

Here we calculate the $\eta_{inj\_QW\_above\_th}$, from Eq. (18), for 1300 nm InGaAsN QW lasers utilizing various barrier regions. The calculation of $\eta_{inj\_QW\_above\_th}$ here assumes an

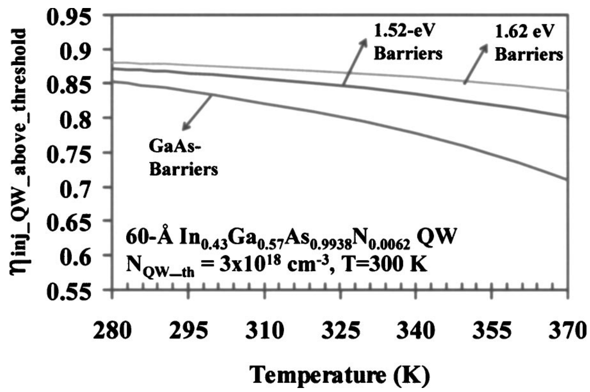

FIG. 16. The $\eta_{\text{inj\_QW\_above\_th}}$ for InGaAsN QW lasers with various barriers, as a function of temperature.

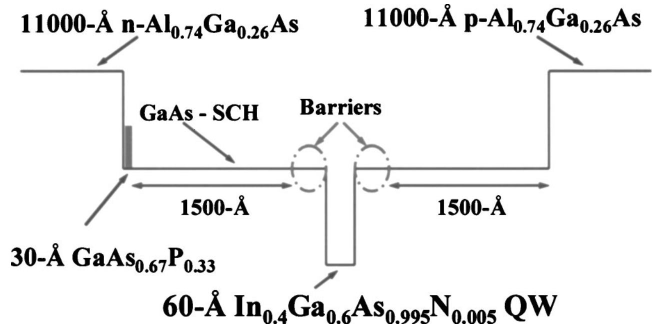

FIG. 17. Cross sectional schematic band diagram of InGaAsN QW lasers.

unclamping rate (Δ_{QW}) of 11%. The purpose of the analysis here is not to attempt to calculate an accurate value for $\eta_{\text{inj\_QW\_above\_th}}$, rather it is to provide the trend of the temperature characteristics of $\eta_{\text{inj\_QW\_above\_th}}$ for InGaAsN QW lasers with improved carrier confinement in the QW. The utilization of larger band gap barriers of 1.52 or 1.62 eV InGaAsP surrounding the 1300 nm InGaAsN QW will provide significantly improved carrier confinement to the QW. As shown in Figs. 16, the $\eta_{\text{inj\_QW\_above\_th}}$ for the InGaAsN QW with GaAs barriers exhibits large temperature sensitivity, resulting in low $\eta_{\text{inj\_QW\_above\_th}}$ at elevated temperature. In contrast to the case for GaAs barriers, the $\eta_{\text{inj\_QW\_above\_th}}$ for the InGaAsN QW with larger band gap barriers of 1.52 and 1.62 eV InGaAsP exhibit only very minimal temperature sensitivity, which potentially lead to significant reduction of the temperature sensitivity of the external differential quantum efficiency (η_d). The experimental results presented in Sec. VIII also show a similar trend of significant reduction in temperature sensitivity of η_d for the InGaAsN QW lasers utilizing larger band gap barrier materials.

VIII. EXPERIMENTAL VERIFICATION OF THE CARRIER LEAKAGE EFFECT

A. Design of experiments and structures

Here we conduct experiments to demonstrate the existence of the temperature-induced carrier leakage in InGaAsN QW lasers. This work shows that carrier leakage in InGaAsN QW cannot be neglected, despite its deep electron confinement. Experiments are designed carefully, in which only the choice of the barriers surrounding an identical InGaAsN QW are modified from the conventional GaAs barriers to higher band gap $GaAs_{1-x}P_x$ barriers, as shown in Fig. 17 and 18.

By replacing only the choice of the barrier material surrounding the InGaAsN QW directly (i.e., sometimes we refer to this as the direct barrier), the thermionic escape lifetime of the carriers in the QW will be altered as a consequence of changes in the band offsets (ΔE_b). In our experiments with larger band gap barriers, we utilize the $GaAs_{0.85}P_{0.15}$ and $GaAs_{0.67}P_{0.33}$ barriers surrounding the QW directly. By utilizing the GaAsP direct barriers, significant suppression of the carrier leakage phenomena at elevated temperature is observed, resulting in the realization of InGaAsN QW lasers with low J_{th} and improved T_0 values at elevated temperatures. It is also important to note that the improvement in T_0 values in the InGaAsN–GaAsP laser structure is not a result of an artificial increase in the J_{th}.

The J_{th} of QW lasers can be expressed as a function of device parameters, which include total recombination current in the QW ($J_{\text{th\_QW}}$) and the current injection efficiency ($\eta_{\text{inj\_QW\_at\_th}}$) as follows:

$$J_{\text{th}} = \frac{qL_z}{\eta_{\text{inj\_at\_th}}} \cdot (A_{\text{QW}}N_{\text{QW}} + B_{\text{QW}}N_{\text{QW}}^2 + C_{\text{QW}}N_{\text{QW}}^3), \qquad (26)$$

with $J_{\text{th\_QW}}=qL_z(AN_{\text{QW}}+BN_{\text{QW}}^2+CN_{\text{QW}}^3)$. The q, L_z, and N_{QW} in Eq. (26) represent the electron charge, thickness of the QW, and carrier density in the QW, respectively. The A_{QW}, B_{QW}, and C_{QW} represent the monomolecular, bimolecular, and Auger recombination coefficients, respectively, as discussed in Sec. IV D. The temperature sensitivity of $\eta_{\text{inj\_at\_th}}$ in InGaAsN QW lasers, as shown in Sec. VI and Eq. (14), can be improved by utilizing the larger band gap barrier materials to suppress the thermionic carrier leakages. The expression for $\eta_{\text{inj\_QW\_at\_th}}$ of QW lasers is shown in Eq. (14) as functions of τ_{bw} (total carrier transport time), τ_b (total recombination lifetime in the SCH region), $\tau_{\text{QW\_total}}$ (total recombination lifetime in the QW active region), and τ_e (thermionic carrier escape lifetime). The expression in Eq. (14) can be derived from the conventional rate equation for QW lasers, as shown in Sec. III. All the parameters of interest (τ_{bw}, τ_b, $\tau_{\text{QW\_total}}$, and τ_e) have been discussed in detail in Secs. IV and V. The τ_{bw} and τ_b are assumed as unchanged in all our experiments, as the design and the choice of material sys-

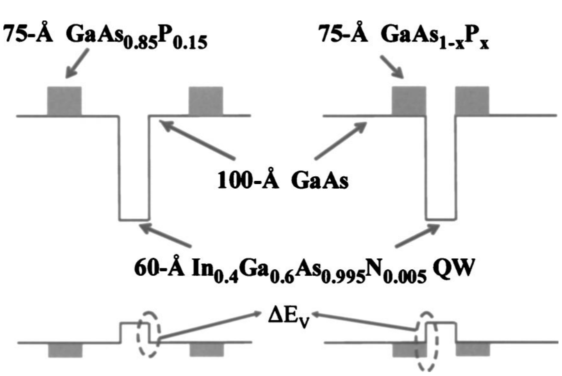

FIG. 18. Diagram of the InGaAsN QW with direct barriers of: (a) GaAs and (b) $GaAs_{1-x}P_x$.

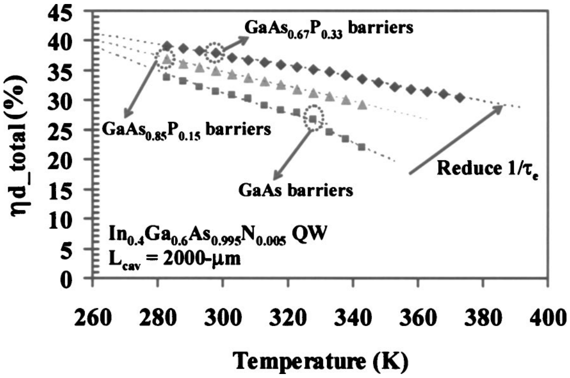

FIG. 19. The η_d for InGaAsN QW lasers with various barriers as a function of T.

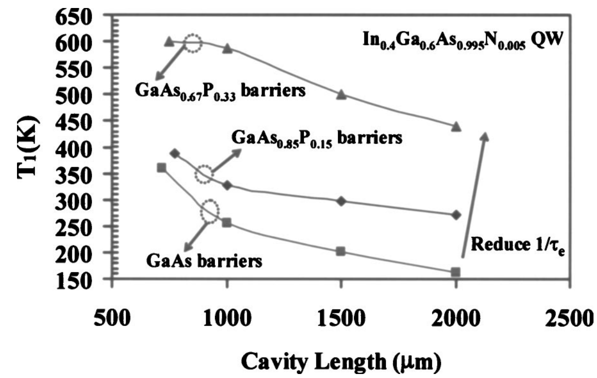

FIG. 20. The T_1 for InGaAsN QW lasers with various barriers, as a function of L_{cav}.

tems of the SCH region are identical for all structures investigated here. From the fact that the compositions and dimensions of the InGaAsN QW active regions in both experiments are kept identical, the total recombination lifetime in the QW $\tau_{\mathrm{QW\_total}}$ can also be assumed as unchanged.

The thermionic carrier escape lifetime ($\tau_{e\_e,h}$ for electrons and holes, respectively) of the carriers in the QW have been discussed in detail in Secs. IV C and V, following Eq. (24) and (25). The simple trend of the expression for thermionic carrier escape rate can be expressed as follows:

$$\frac{1}{\tau_{e\_e,h}} \propto \frac{1}{N_{\mathrm{QW}} \cdot L_z} \cdot T^2 \cdot \exp\left(-\frac{\Delta E_{b\_e,h}}{k_B T}\right), \tag{27}$$

with k_B as the Boltzmann constant, T as the temperature, N_{QW} as the carrier density in QW, L_z as the thickness of QW, and $\Delta E_{b\_e,h}$ as the carrier confinement energy in QW (for electrons and holes, respectively). As the dimension (L_z) and composition of the InGaAsN QW active region in both experiments are identical, the threshold carrier density in the QW ($N_{\mathrm{QW\_th}}$) can also be assumed as identical for both lasers with similar confinement and cladding layer designs. The total thermionic carrier escape time of QW (τ_e) can be expressed as functions of the $\tau_{e\_\mathrm{electron}}$ and τ_{e_holes} as $1/\tau_e = 1/\tau_{e\_\mathrm{electron}} + 1/\tau_{e\_\mathrm{holes}}$. The escape phenomenon is dominated by the escape rate of the carriers with the fastest escape time. Once the carriers escape, the carriers in the QW and SCH will redistribute themselves to maintain charge neutrality in the QW and SCH due to the high mobility of the carriers.[16,34]

The differences in the τ_e of InGaAsN–GaAs and InGaAsN–GaAsP structures can be attributed solely to the differences in their respective ratios of $\Delta E_{b\_e,h}/k_B T$. The ratios of the electron and hole confinement energy ($\Delta E_c : \Delta E_v$, with $\Delta E_c = \Delta E_{b\_e}$, $\Delta E_v = \Delta E_{b\_h}$) in InGaAsN–GaAs structures is approximately 80:20,[19,20] resulting in extremely strong electron confinement and extremely poor heavy hole confinement. The calculated escape lifetime of the electrons and holes from InGaAsN QW is approximately 30–50 ns and 5–10 ps, respectively, for near-threshold conditions.[16,34] By utilizing the large band gap material surrounding the InGaAsN QW, the confinement energy of both the electrons and holes in the QW will be increased. As no studies have been reported on the InGaAsN–GaAsP structures, the $\Delta E_c : \Delta E_v$ ratio is assumed to be similar to that of the InGaAsN–GaAs case. A slight increase in ΔE_v leads to significant suppression of hole escape rate ($1/\tau_e$) from the InGaAsN–GaAsP QW structures due to its exponential relation [from Eq. (27)], which will in turn lead to improved η_{inj} and J_{th} at elevated temperatures [from Eq. (14) and (27)]. In the absence of any carrier leakage, by contrast, an increase in ΔE_v will not lead to any reduction in J_{th} at elevated temperatures or any improvement in the T_0 values.

All laser structures studied here, shown in Figs. 17 and 18, were grown by low-pressure MOCVD. The group-V precursors are arsine (AsH_3) and phosphine (PH_3). The group-III precursors are the trimethyl (TM) sources of Ga, Al, and In. The N precursor is U dimethylhydrazine (U-DMHy). The dopant sources are SiH_4 and dielthylzinc (DEZn) for the n and p dopants, respectively. Details of the MOCVD growth of InGaAsN QW materials utilizing GaAs barriers and larger band gap materials of GaAsP have been discussed elsewhere in Refs. 3, 4, and 47.

B. Lasing characteristics of InGaAsN QW lasers

As-cleaved broad area lasers, with oxide-defined stripe width of 100 μm, were fabricated for both active regions shown in Figs. 19–22. The lasing characteristics were measured under pulsed conditions with a pulse width and a duty cycle of 5 μs and 1%, respectively. The temperature characterizations of both InGaAsN–GaAsP and InGaAsN–GaAs QWs lasers are performed over the range of 10–100 °C. The

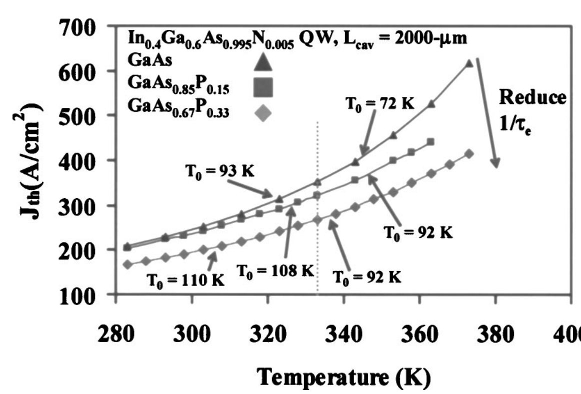

FIG. 21. The J_{th} for InGaAsN QW lasers with various barriers, as a function of T.

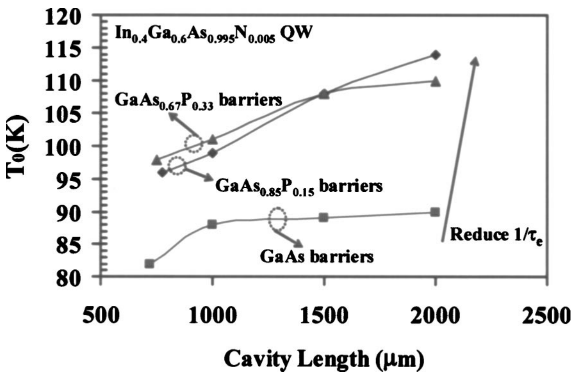

FIG. 22. The T_0 for InGaAsN QW lasers with various barriers, as a function of L_{cav}.

measurement is conducted for devices with long cavity to minimize the effect from the temperature sensitivity of material gain.[15] The T_0 and T_1 values presented in Figs. 20 and 21 are measured for devices with various cavity lengths from temperature ranges of 20–60 °C.

The emission wavelengths of the InGaAsN QW lasers (L_{cav}=2000 μm) with $GaAs_{0.85}P_{0.15}$ and $GaAs_{0.67}P_{0.33}$ barriers are approximately 1280 and 1260 nm, respectively. The emission wavelength of the InGaAsN–GaAs QW laser structure is measured as 1295 nm. The shorter peak emission wavelength from the InGaAsN QW with direct barriers of GaAsP is a result of a stronger quantum confinement effect as well as growth-to-growth variation in composition. Calculations considering the band gap, strain, and effective masses predict a blueshift of the emission wavelength of approximately 120–300 Å for InGaAsN–GaAsP QW structures, in close agreement with experiments.

The temperature characteristics of the external differential quantum efficiencies (η_d) of InGaAsN QW lasers with various barriers are presented in Figs. 19 and 20. The η_d of the InGaAsN QW lasers with GaAs barriers exhibits relatively large temperature sensitivity, resulting in low η_d at elevated temperature. As larger band gap barriers are employed to surround the InGaAsN QW, the η_d exhibit significant reduction of the temperature sensitivity of its η_d. The utilization of the GaAsP barriers results in the reduction of the $1/\tau_{e\_heavy\_holes}$ (thermionic escape rate for heavy holes), which will in turn result in significant reduction in the temperature sensitivity of its $\eta_{inj\_QW\_above\_th}$. Low temperature sensitivity of the $\eta_{inj\_QW\_above\_th}$ is crucial for the realization of QW lasers with reduced temperature sensitivity of η_d. The measured temperature characteristics of the η_d with increasing carrier confinement in Fig. 19 exhibit a very similar trend with that of the $\eta_{inj\_QW\_above\_th}$ in Fig. 16, which can be explained by their linear relation shown in Eq. (5). As shown in Fig. 20, the T_1 values for InGaAsN QW lasers with improved carrier confinement in the QW, exhibit significant improvement in the T_1 values for various cavity lengths. T_1 values of approximately 450 K are measured for long-cavity devices employing $GaAs_{0.67}P_{0.33}$ barriers, which is significantly higher than that (T_1=150 K) measured for devices with GaAs barriers.

The threshold current densities (J_{th}) of InGaAsN QW lasers with GaAs barriers and larger band gap barriers of GaAsP are shown in Figs. 21 and 22. At room temperature (T=20 °C), threshold characteristics of both the InGaAsN–GaAs are measured as approximately 350–360, 250, and 210–220 A/cm^2, for devices with cavity lengths of 720, 1000, and 2000 μm, respectively. Room-temperature (T=20 °C) threshold current densities of 320, 260, and 220 A/cm^2 were measured for InGaAsN–$GaAs_{0.85}P_{0.15}$ QW lasers for cavity lengths of 775, 1000, and 2000 μm, respectively. The J_{th} for the InGaAsN–$GaAs_{0.67}P_{0.33}$ QW lasers is measured as 200 A/cm^2 for devices with L_{cav}=2000 μm.

Threshold current densities for InGaAsN QW lasers, with GaAs and GaAsP barriers, exhibit similar values (J_{th}=200–220 A/cm^2) for room-temperature (T=20 °C) measurements. At elevated temperature, the J_{th} of InGaAsN QW lasers with GaAs barriers exhibit large temperature sensitivity resulting in J_{th} of 535 and 625 A/cm^2 at temperatures of 90 and 100 °C, respectively. Threshold current densities of only 390 and 440 A/cm^2 were also measured for InGaAsN–$GaAs_{0.85}P_{0.15}$ QW lasers (L_{cav}=2000 μm) at temperatures of 80 and 90 °C, respectively. Further suppression of carrier leakages, by utilizing the GaAsP barriers, results in InGaAsN–$GaAs_{0.85}P_{0.15}$ QW lasers (L_{cav}=2000 μm) with threshold current densities of only 350 and 400 A/cm^2 at temperatures of 90 and 100 °C, respectively. As shown in Fig. 22, T_0 values for the InGaAsN QW lasers, with GaAsP barriers for various cavity lengths, also exhibit improved characteristics in comparison to those of InGaAsN–GaAs QW lasers. The improvement in the T_0 values for the QW lasers with larger band gap barriers is a result of significant suppression of thermionic carrier leakage.

As electrons are very well confined in both InGaAsN QW laser structures, the reduction of the J_{th} of the InGaAsN–GaAsP QW structures at elevated temperatures as well as their improved T_0 and T_1 values are results of suppression of heavy hole leakage from the InGaAsN QW due to the lower hole escape rate ($1/\tau_{e\_hole}$). As the temperature increases, the J_{th} of the InGaAsN with GaAsP barriers increases at a significantly slower rate. The suppression of carrier leakage is also evident from the fact that the significantly reduced temperature sensitivity of η_d in the InGaAsN QW lasers employs larger band gap barrier materials.

From the studies presented here, the existence of carrier leakage in InGaAsN QW lasers has been demonstrated experimentally. Suppression of carrier leakage in InGaAsN QW lasers with larger band gap barrier material of GaAsP leads to a reduction in the J_{th} at elevated temperature, accompanied by the increase in the T_0 and T_1 values. The J_{th} of the InGaAsN QW lasers (L_{cav}=2000 μm, as-cleaved), with $GaAs_{0.67}P_{0.33}$ direct barriers, have been measured as only 350 and 400 A/cm^2, for measurements at temperature of 90 and 100 °C, respectively. Suppression of the carrier leakage in InGaAsN QW lasers also results in significant reduction in the temperature sensitivity of the slope efficiency (η_d) for the structures employing large band gap of GaAsP.

IX. SUMMARY

The analysis of the current injection efficiency here indicates that the at-threshold ($\eta_{inj\_QW\_at\_th}$) and above-threshold ($\eta_{\text{inj\_QW\_above\_th}}$) current injection efficiency of QW lasers can be very distinct, something which is generally overlooked in the diode laser literature. The threshold current density of QW lasers is controlled by the injection efficiency at threshold, and not by the above-threshold injection efficiency. The severe thermionic carrier leakage from the QW to the barrier region will significantly lead to severe reductions of the below-threshold ($\eta_{\text{inj\_QW\_below\_th}}$) and at-threshold ($\eta_{\text{inj\_QW\_at\_th}}$) current injection efficiency at elevated temperature. Only when carriers in the QW are fully clamped ($\Delta_{\text{QW}}=0$) and the thermionic carrier escape rate is completely negligible ($1/\tau_e \to 0$), can the above-threshold and below-threshold current injection efficiency be equal. In contrast to the common understanding, the $\eta_{\text{inj\_QW\_at\_th}}$ of QW lasers increases as the nonradiative recombination in the QW is increased, attributed to the faster recombination lifetime of the carriers in the QW. The $\eta_{\text{inj\_QW\_at\_th}}$ of QW lasers with larger nonradiative recombination, have also been shown to be less temperature sensitive, attributed to the reduced τ_{QW}/τ_e ratio. From our analysis, the below-threshold current injection efficiency of the QW laser is a strong function of the carrier density in QW, temperature, and band offset of the QW barrier region. The method of extracting the $\eta_{\text{inj\_QW\_above\_th}}$ by utilizing the multiple length studies of QW laser devices is valid, as the $\eta_{\text{inj\_QW\_above\_th}}$ is almost constant for the N_{QW} values near threshold ($N_{\text{QW}} \sim 1-7 \times 10^{18}\ \text{cm}^{-3}$).

Here we demonstrate that it is crucial to take into account the carrier leakage in InGaAsN QW lasers, despite its deep electron confinement. We have also found that the higher temperature sensitivity of the threshold current of 1300 nm InGaAsN QW lasers, compared to the case for 1200 nm InGaAs QW, can be explained from the significantly larger thermionic carrier spillover from the QW to the SCH region, which will in turn lead to the reduction of the at-threshold current injection efficiency of InGaAsN QW lasers and a larger temperature dependence. Just from the fact that the $\eta_{\text{inj\_QW\_at\_th}}$ of the InGaAsN QW is significantly reduced even at room temperature, the threshold current density of InGaAsN QW lasers is predicted to increase significantly, in agreement with experiment. The thermionic carrier spillover in InGaAsN QW is governed by the poor heavy-hole confinement. Design analysis utilizing MQW structures with direct barriers of GaAsP outer barriers and GaAs(N) barriers, should allow reduced temperature sensitivity of the at-threshold current injection efficiency of InGaAsN QW lasers. Experimental evidence of the existence of carrier leakage is obtained by utilizing large band gap barriers of GaAsP to surrounding the InGaAsN QW, which in turn results in a significant suppression of the thermionic carrier escape at elevated temperatures. Aside from the carrier leakage effect, we also find that the higher temperature sensitivity of the material gain parameter in InGaAsN might also be a significant factor in leading to the lower T_0 values observed (compared with InGaAs).[1]

ACKNOWLEDGMENT

The authors would like to acknowledge helpful discussion on the topic of current injection efficiency of quantum well lasers with Professor Peter Blood (Cardiff University), Dr. Peter Smowton (Cardiff University), Professor Peter S. Zory (University of Florida), and Professor Dan Botez (University of Wisconsin-Madison). The authors would like to greatly acknowledge contributions from Jeng-Ya Yeh of the University of Wisconsin-Madison on parts of the experimental aspects of the works.

[1] N. Tansu and L. J. Mawst, IEEE Photonics Technol. Lett. **14**, 1052 (2002).
[2] R. Fehse, S. Tomic, A. R. Adams, S. J. Sweeney, E. P. O'Reilly, A. Andreev, and H. Riechert, IEEE J. Sel. Top. Quantum Electron. **8**, 801 (2002).
[3] N. Tansu and L. J. Mawst, IEEE Photonics Technol. Lett. **14**, 444 (2002).
[4] N. Tansu, N. J. Kirsch, and L. J. Mawst, Appl. Phys. Lett. **81**, 2523 (2002).
[5] W. Ha, V. Gambin, M. Wistey, S. Bank, S. Kim, and J. S. Harris, Jr., IEEE Photonics Technol. Lett. **14**, 591 (2002).
[6] K. D. Choquette *et al.*, Electron. Lett. **36**, 1388 (2000).
[7] M. Kawaguchi, T. Miyamoto, E. Gouardes, D. Schlenker, T. Kondo, F. Koyama, and K. Iga, Jpn. J. Appl. Phys., Part 2 **40**, L744 (2001).
[8] F. Hohnsdorf, J. Koch, S. Leu, W. Stolz, B. Borchert, and M. Druminski, Electron. Lett. **35**, 571 (1999).
[9] C. S. Peng, T. Jouhti, P. Laukkanen, E.-M. Pavelescu, J. Konttinen, W. Li, and M. Pessa, IEEE Photonics Technol. Lett. **14**, 275 (2002).
[10] D. A. Livshits, A. Yu. Egorov, and H. Riechert, Electron. Lett. **36**, 1381 (2000).
[11] T. Takeuchi, Y.-L. Chang, M. Leary, A. Tandon, H.-C. Luan, D. P. Bour, S. W. Corzine, R. Twist, and M. R. Tan, Proceedings IEEE LEOS 2001 Post-Deadline Session, San Diego, November 2001.
[12] J. Wei, F. Xia, C. Li, and S. R. Forrest, IEEE Photonics Technol. Lett. **14**, 597 (2002).
[13] N. Tansu, A. Quandt, M. Kanskar, W. Mulhearn, and L. J. Mawst, Appl. Phys. Lett. **83**, 18 (2003).
[14] N. Tansu and L. J. Mawst, IEEE Photonics Technol. Lett. **13**, 179 (2001).
[15] N. Tansu, Y. L. Chang, T. Takeuchi, D. P. Bour, S. W. Corzine, M. R. T. Tan, and L. J. Mawst, IEEE J. Quantum Electron. **38**, 640 (2002).
[16] N. Tansu, J. Y. Yeh, and L. J. Mawst, Appl. Phys. Lett. **83**, 2112 (2003).
[17] N. Tansu, J. Y. Yeh, and L. J. Mawst, Proceedings of the IEEE/OSA Conference on Lasers and Electro-Optics (CLEO) 2003, Baltimore, MD, June 2003, Paper CTuH4.
[18] P. M. Smowton and P. Blood, IEEE J. Sel. Top. Quantum Electron. **3**, 491 (1997).
[19] G. P. Agrawal and N. K. Dutta, *Semiconductor Lasers* (Van Nostrand, New York, 1993).
[20] S. L. Chuang, *Physics of Optielectronic Devices* (Wiley, New York, 1995).
[21] L. A. Coldren and S. W. Corzine, *Diode Lasers and Photonics Integrated Circuits* (Wiley, New York, 1995).
[22] W. W. Chow and S. W. Koch, *Semiconductor-Lasers Fundamentals* (Springer, Berlin, 1999).
[23] R. Nagarajan and J. E. Bowers, IEEE J. Quantum Electron. **29**, 1601 (1993).
[24] K. Y. Lau and A. Yariv, *Semiconductors and Semimetals: Lightwave Communications Technology*, edited by R. K. Willardson and A. C. Beers (Academic, New York, 1985), Vol. 22B.
[25] R. Nagarajan, M. Ishikawa, T. Fukushima, R. S. Geels, and J. E. Bowers, IEEE J. Quantum Electron. **28**, 1990 (1992).
[26] K. Y. Lau, "Dynamics of quantum well lasers," in *Quantum Well Lasers*, edited by P. S. Zory, Jr. (Academic, New York, 1993).
[27] G. W. Taylor and S. Jin, IEEE J. Quantum Electron. **34**, 1886 (1998).
[28] M. P. Kessler, C. S. Harder, and E. E. Latta, Appl. Phys. Lett. **59**, 2775 (1991).
[29] W. Liu, *Fundamental of III-V Devices: HBTs, MESFETs, and HFETs/HEMTs* (Wiley, New York, 1999).
[30] D. Sunderland and P. D. Dapkus, IEEE Trans. Electron Devices **34**, 367 (1987).
[31] S. M. Sze, *Physics of Semiconductor Devices* (Wiley, New York, 1981).
[32] H. Schneider and K. V. Klitzing, Phys. Rev. B **38**, 6160 (1988).
[33] M. Irikawa, T. Ishikawa, T. Fukushima, H. Shimizu, A. Kasukawa, and K. Iga, Jpn. J. Appl. Phys., Part 1 **39**, 1730 (2000).
[34] N. Tansu and L. J. Mawst, Appl. Phys. Lett. **82**, 1500 (2003).
[35] N. Tansu, J. Y. Yeh, and L. J. Mawst, Appl. Phys. Lett. **83**, 2112 (2003).

[36] H. A. Bethe, MIT Radiat. Lab. Rep. **43**, 12 (1942).
[37] W. W. Chow, E. D. Jones, N. A. Modine, A. A. Allerman, and S. R. Kurtz, Appl. Phys. Lett. **75**, 2891 (1999).
[38] M. Hetterich, M. D. Dawson, A. Yu. Egorov, D. Bernklau, and H. Riechert, Appl. Phys. Lett. **76**, 1030 (2000).
[39] B. Jogai, Appl. Phys. Lett. **59**, 1329 (1991).
[40] J. J. Coleman, "Strained layer quantum well heterostructure lasers," in *Quantum Well Lasers*, edited by P. S. Zory, Jr. (Academic, New York, 1993).
[41] S. W. Corzine, R. H. Yan, and L. A. Coldren, Appl. Phys. Lett. **57**, 2835 (1990).
[42] S. Niki, C. L. Lin, W. S. C. Chang, and H. H. Wieder, Appl. Phys. Lett. **55**, 1339 (1989).
[43] J. B. Heroux, C. Yang, and W. I. Wang, J. Appl. Phys. **92**, 4361 (2002).
[44] J. C. L. Yong, J. M. Rorison, and I. H. White, Appl. Phys. Lett. **79**, 1085 (2001).
[45] A. F. Phillips, A. F. Sweeney, A. R. Adams, and P. J. A. Thijs, IEEE J. Sel. Top. Quantum Electron. **5**, 401 (1999).
[46] D. A. Ackerman, P. A. Morton, G. E. Shtengel, M. S. Hybertsen, R. F. Kazarinov, T. Tanbun-Ek, and R. A. Logan, Appl. Phys. Lett. **66**, 2613 (1995).
[47] N. Tansu, J. Y. Yeh, and L. J. Mawst, Appl. Phys. Lett. **82**, 3008 (2003).
[48] G. Lim, Y. Park, C. A. Zmudzinski, P. S. Zory, L. M. Miller, T. L. Cockerill, J. J. Coleman, C. S. Hong, and L. Figueroa, Proc. SPIE **1418**, 123 (1991).